Cell Stem Cell

Article

Space-associated stem cell hallmarks of aging and resilience in astronauts

Graphical abstract

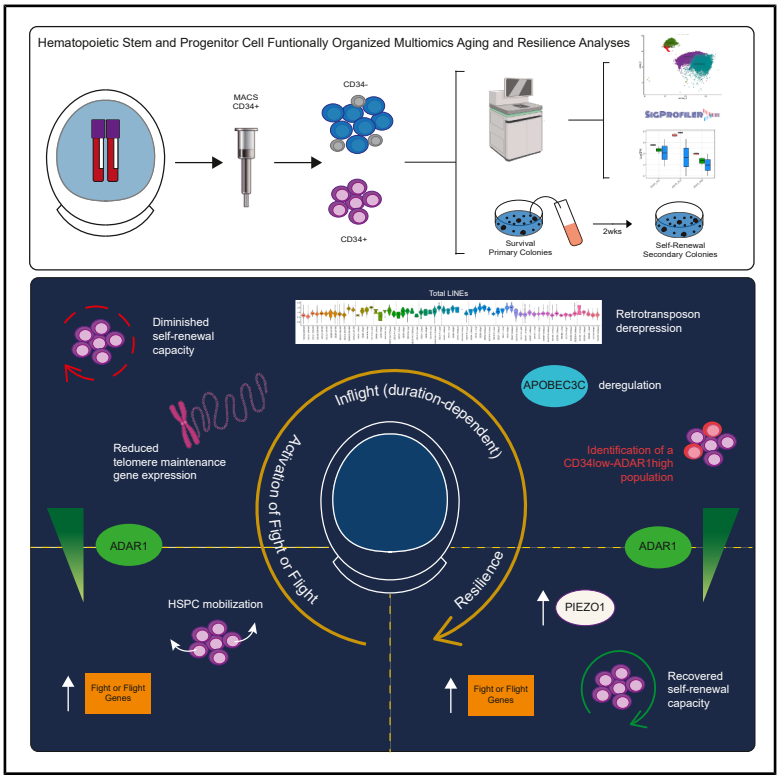

Highlights

- Spaceflight altered HSPC cycle, self-renewal, and immune repertoires
- Spaceflight altered HSPC telomere, mitochondrial, and cytokine regulation
- Spaceflight induced HSPC mutations, base deaminase, and retrotransposon deregulation
- These analyses revealed functional and molecular hallmarks of stem cell resilience

Authors

Jessica Pham, Shuvro P. Nandi, Larisa Balaian, ..., Thomas Whisenant, Ludmil B. Alexandrov, Catriona H.M. Jamieson

Correspondence

cjamieson@health.ucsd.edu

In brief

Hematopoietic stem and progenitor cell functionally organized multi-omics aging and resilience (HSPC-FOMA-R) analyses of 9 astronauts before, during, and after ISS missions revealed hallmarks of accelerated aging, including reduced self-renewal and telomere maintenance, mitochondrial dysfunction, and genomic instability with clonal mutations together with cytokine and retrotransposon deregulation.

Pham et al., 2025, Cell Stem Cell *32*, 1–18
December 4, 2025
https://doi.org/10.1016/j.stem.2025.11.001

CellPress

Please cite this article in press as: Pham et al., Space-associated stem cell hallmarks of aging and resilience in astronauts, Cell Stem Cell (2025), https://doi.org/10.1016/j.stem.2025.11.001

Cell Stem Cell

CellPress
OPEN ACCESS

Article

Space-associated stem cell hallmarks of aging and resilience in astronauts

Jessica Pham,[1] Shuvro P. Nandi,[2,3] Larisa Balaian,[1] Claire Engstrom,[1] Patrick Chang,[1] Karla Mack,[1] Inge van der Werf,[1] Emma Klacking,[1] Jenna Sneifer,[1] Neha Katragadda,[1] Kendale Wirtjes,[1] Antonio Ruiz,[1] Daisy Chilin-Fuentes,[4] Elsa Molina,[5] Pinar Mesci,[6] Jana Stoudemire,[1] Sheldon R. Morris,[1] Thomas Whisenant,[4] Ludmil B. Alexandrov,[1,2,3] and Catriona H.M. Jamieson[1,7,*]

[1]Sanford Stem Cell Institute, Division of Regenerative Medicine, Department of Medicine, University of California, San Diego, La Jolla, CA, USA
[2]Department of Cellular and Molecular Medicine, University of California, San Diego, La Jolla, CA, USA
[3]Department of Bioengineering, University of California, San Diego, La Jolla, CA, USA
[4]Center for Computational Biology and Bioinformatics, University of California, San Diego, La Jolla, CA, USA
[5]Next Generation Sequencing Core, The Salk Institute for Biological Studies, La Jolla, CA, USA
[6]Axiom Space, Houston, TX, USA
[7]Lead contact
*Correspondence: cjamieson@health.ucsd.edu
https://doi.org/10.1016/j.stem.2025.11.001

SUMMARY

Previous reports revealed immune dysfunction, chromosomal abnormalities, cytokine deregulation, and telomere alterations after prolonged spaceflight. However, the stress of space on hematopoietic stem and progenitor cells (HSPCs) and the resilience properties maintaining lifelong hematopoiesis and immunity were not studied. We performed HSPC functionally organized multi-omics aging and resilience (HSPC-FOMA-R) analyses in 9 astronauts before, during, and after three short-duration International Space Station (ISS) missions. Whole-genome sequencing (with telomere length analysis and mitochondrial and clonal mutational profiling), whole-transcriptome sequencing (with RNA editing and retrotransposon analyses), single-cell RNA sequencing, cytokine arrays, and fluorescence-activated cell sorting (FACS) analyses assessed HSPC and immune subpopulation survival dynamics. We show that spaceflight is associated with partially reversible changes in HSPC survival and self-renewal, adenosine deaminase associated with RNA1 (ADAR1), telomere maintenance, mobilization, cell cycle, and "fight or flight" gene expression. Combined with clonal hematopoietic mutations, apolipoprotein B mRNA editing catalytic polypeptide-like (APOBEC3C) activation, and retrotransposon deregulation, HSPC-FOMA-R analyses are needed before extended missions.

INTRODUCTION

Lifelong blood cell production and effective immune responses are predicated on the maintenance of healthy hematopoietic stem cells (HSCs) that can reside dormant in protective niches, mobilize following a "fight or flight" response, self-renew (regenerate), and differentiate into all blood cell types.[1–8] Hallmarks of stem cell aging include reduced self-renewal capacity, loss of dormancy, increased mobilization from bone marrow niches, telomere attrition and reduced telomere maintenance, genomic instability, mitochondrial stress, accumulation of clonal mutations,[9,10] and retrotransposon derepression,[11] which triggers interferon-related inflammation-associated aging (inflammaging).[1,12–14] These hallmarks of stem cell aging can be acquired in response to chronic or acute macroenvironmental exposures or stressors.[1,4,15,16]

Pioneering astronaut research, including the National Aeronautics and Space Administration (NASA) Twins Study from a 1-year-long mission and The Space Omics and Medical Atlas (SOMA) studies from short-term missions, has shown that spaceflight serves as a profound stressor, capable of reshaping the immune system,[17–19] altering physiologic function,[20] and causing prolonged molecular and cellular changes in many tissues.[21] Moreover, NASA research utilizing animal models, simulated microgravity, and human-derived cell cultures has revealed changes in inflammatory cytokines and shifts in immune cell populations typical of aging.[18,19,22–25] Previously, we investigated whether immune deficits arise from hematopoietic stem and progenitor cell (HSPC) dysfunction in space in 4 one-month-long NASA-supported integrated space stem cell orbital research (ISSCOR) center (SpX-24, SpX-25, SpX-26, and SpX-27) missions to the International Space Station (ISS) that utilized novel AI-driven 3D nanobioreactors seeded with aged normal bone marrow-derived HSPCs and stromal cells.[26] In these ISSCOR studies, we observed niche-dependent HSPC dysfunction following post-spaceflight return compared with ground-based

Please cite this article in press as: Pham et al., Space-associated stem cell hallmarks of aging and resilience in astronauts, Cell Stem Cell (2025), https://doi.org/10.1016/j.stem.2025.11.001

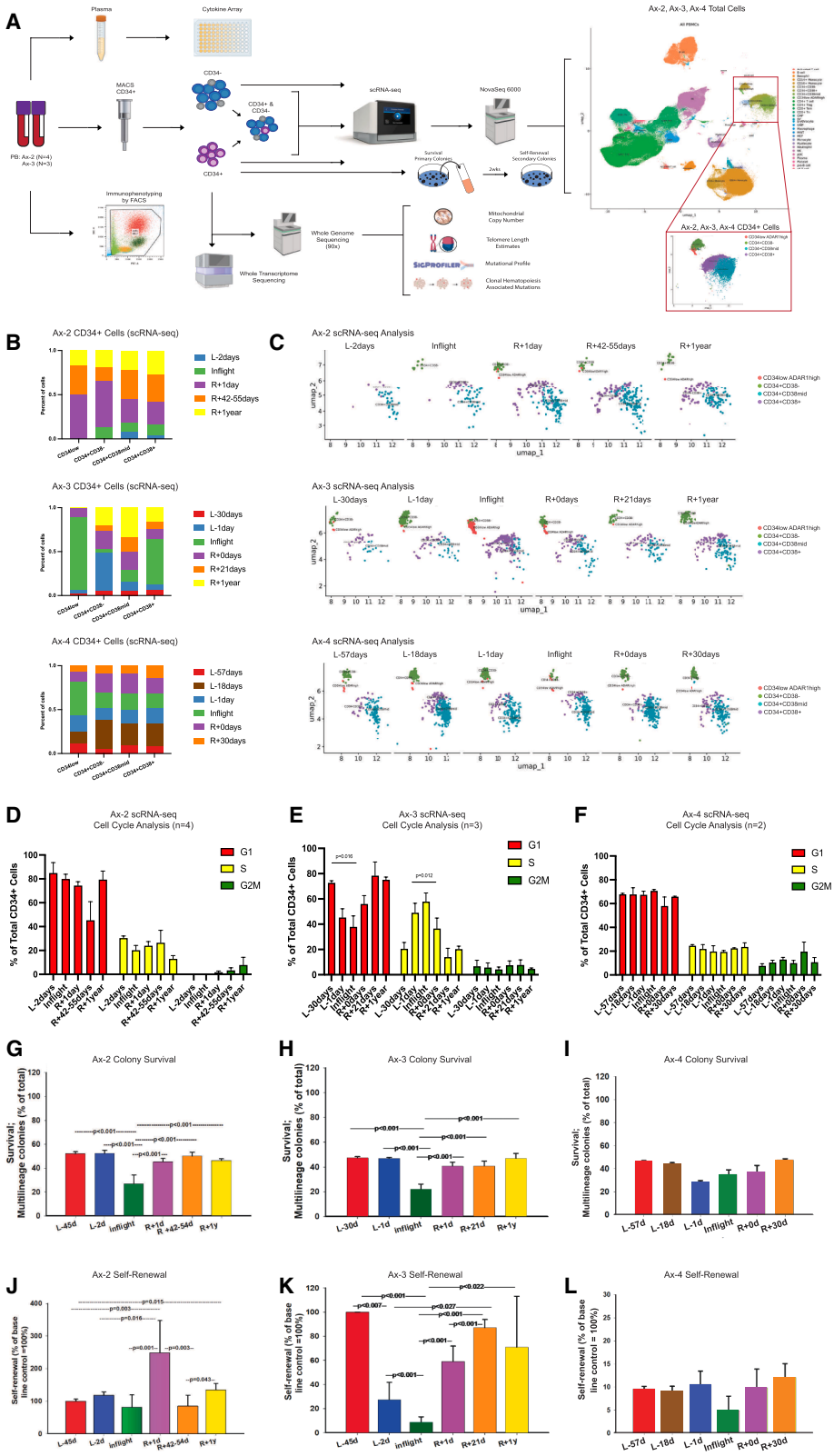

Figure 1. HSPC-FOMA-R analyses of astronauts

(A) Experimental design of HSPC-FOMA-R analyses of astronauts. In sequential studies, HSPCs were isolated from astronaut peripheral blood before, during, and after the Ax-2, Ax-3, and Ax-4 missions to the ISS. Whole peripheral blood was returned within 96 h of collection on ice and immediately processed by density

(legend continued on next page)

Please cite this article in press as: Pham et al., Space-associated stem cell hallmarks of aging and resilience in astronauts, Cell Stem Cell (2025), https://doi.org/10.1016/j.stem.2025.11.001

controls, which included reduced HSPC self-renewal capacity, base deaminase deregulation, reduced telomere maintenance gene expression, and dynamic retrotransposon derepression. Although we observed significant effects of spaceflight from *in vitro* nanobioreactor models of human HSPC aging, the temporal sequence and long-term impact of space-associated stem cell hallmarks of aging and resilience (SASHA-R) in astronauts had not been addressed to date.

To investigate the direct functional and molecular impact of spaceflight as a macroenvironmental stressor, we performed the first sequential astronaut HSPC functionally organized multi-omics aging and resilience (HSPC-FOMA-R) analyses before, during, and after 10-, 21-, and 20-day Axiom (Ax-2, Ax-3, and Ax-4) private astronaut missions (PAMs) to the ISS. Overall, HSPC-FOMA analyses revealed space-associated hallmarks of astronaut aging, including significant cell cycle alterations, decreased self-renewal capacity, genomic instability typified by clonal mutations together with the HSPC mobilization gene, altered telomere maintenance, retrotransposons, inflammatory cytokines, and adenosine deaminase associated with RNA1 (ADAR1) and apolipoprotein B mRNA editing catalytic polypeptide-like (APOBEC3C) base deaminase deregulation.

RESULTS

HSPC-FOMA-R analyses of astronauts

To determine the combined functional and molecular impact of 10-, 21-, and 20-day missions to the ISS in four Ax-2, three Ax-3, two Ax-4 astronauts, and one Ax-4 ground control, we performed a longitudinal study involving sequential acquisition of 10 mL of peripheral blood, in accordance with NASA Institutional Review Board (IRB)-approved protocols. Blood samples were collected for the Ax-2 crew at launch −45 days (L−45 days), launch −2 days (L−2 days), inflight (prior to hatch closure), return +1 day (R+1 day), return +42–55 days (R+42–55 days), and return +1 year (R+1 year). For the Ax-3 crew, samples were collected at launch −30 days (L−30 days), launch −1 day (L−1 day), inflight (prior to hatch closure), return +0 days (R+0 days), return +21 days (R+21 days), and return +1 year (R+1 year). For the Ax-4 crew, samples were collected at launch −57 days (L−57 days), launch −18 days (L−18 days), launch −1 day (L−1 day), inflight (prior to hatch closure), return +0 days (R+0 days), and return +30 days (R+30 days) (Figures 1A, S1A, and S1B). An additional (n = 1) longitudinal ground control sample was collected during Ax-4 at L−57 days, L−18 days, L−1 day, ground control (at the same time as the inflight collection), and R+1 day (Figure S1G) to gain additional insight into the changes observed in the flight crew samples. Upon arrival at the ISSCOR lab (UC San Diego Sanford Stem Cell Institute, CA) within 24–96 h of venipuncture, peripheral blood mononuclear cells (PBMCs) were isolated by Ficoll Paque followed by immunomagnetic bead purification of $CD34^+$ cells for HSPC-FOMA-R.

For sequential functional analyses of isolated $CD34^+$ cells, we performed colony survival and replating (self-renewal) assays (Ax-2, n = 24; Ax-3, n = 17; Ax-4, n = 12 samples). For multi-omics analyses, we performed $CD34^+$ HSPC-enriched and $CD34^-$ cell whole-genome sequencing (WGS; 90× coverage; Ax-2, n = 47; Ax-3, n = 28; Ax-4, n = 10 samples), telomere length and clonal mutation analyses; $CD34^+$ and $CD34^-$ whole-transcriptome sequencing (RNA sequencing [RNA-seq]; Ax-2, n = 8 samples and 3 time points) with unsupervised hierarchical clustering, gene set enrichment analyses (GSEAs), RNA editing and retrotransposon analyses; and $CD34^+$ versus $CD34^-$ single-cell RNA-seq (scRNA-seq; Ax-2, n = 39; Ax-3, n = 33; Ax-4, n = 24 samples) with uniform manifold approximation and projection (UMAP), GSEA, differential gene expression (DGE) analysis, single-cell transposable element (scTE), and pseudobulk RNA editing analyses. To assess HSPC and immune subpopulation dynamics, we performed fluorescence-activated cell sorting (FACS)-based immunophenotyping (Ax-2, n = 24, and Ax-3, n = 15 samples). To assess inflammatory cytokine production, we performed cytokine arrays for Ax-2 and Ax-3 crew members from plasma at each time point (n = 31) (Figure S1A).

To elucidate HSPC cellular and transcriptomic diversity, we performed scRNA-seq on $CD34^+$ enriched cells using the 10× Genomics 3′ gene expression platform. Samples from all time points between Ax-2, Ax-3, and Ax-4 were integrated and followed by cluster identification[27] using the SingleR and scType algorithms. UMAP of 4,694 $CD34^+$ cells identified four distinct clusters and revealed an increase of $CD34^+$ cells during

centrifugation. Prior to $CD34^+$ cell selection, the mononuclear cell fraction was stained for immunophenotyping analysis by FACS. After $CD34^+$ selection, cells were divided for 90× WGS, scRNA-seq, whole-transcriptome sequencing, and clonogenic survival and self-renewal assays. Diluted plasma was collected for cytokine array analysis.

(B) Stacked bar plots of $CD34^+$ labeled cells by scRNA-seq for Ax-2, Ax-3, and Ax-4. The y axis indicates the percent of cells from each labeled time point. Identified HSPC clusters include $CD34^{low}ADAR1^{high}$, $CD34^+CD38^-$, $CD34^+CD38^{mid}$, and $CD34^+CD38^+$. Ax-2 time points include L−2 days, inflight, R+1 day, R+42–55 days, and R+1 year. Ax-3 time points include L−30 days, L−1 day, inflight, R+0 days, R+21 days, and R+1 year. Ax-4 time points include L−57 days, L−18 days, L−1 day, inflight, R+0 days, and R+30 days.

(C) scRNA-seq UMAP analysis of $CD34^+$ HSPCs from Ax-2 (top), Ax-3 (middle), and Ax-4 (bottom) over time (x axis). Ax-2 time points include (n = 4) L−2 days, inflight, R+1 day, R+42–55 days, and R+1 year. Ax-3 time points include (n = 3) L−30 days, L−1 day, inflight, R+0 days, R+21 days, and R+1 year. Ax-4 time points include (n = 2) L−57 days, L−18 days, L−1 day, inflight, R+0 days, and R+30 days.

(D–F) Bar plots of cell cycle phases (G1, S, G2M) analyzed by scRNA-seq over time of $CD34^+$ cells normalized to total $CD34^+$ cells captured from Ax-2 (D; n = 4), Ax-3 (E; n = 3), and Ax-4 (F; n = 2). Statistical analysis included Student's two-tailed t test. p values less than 0.05 were considered significant.

(G–I) Summarized colony survival data of n = 4 Ax-2 samples (G), n = 3 Ax-3 (H), and n = 2 Ax-4 (I) $CD34^+$ cells. Basal colony formation of original naive untreated cells pre-flight (F; Ax-2 L−45 days; G; Ax-3 L−30 days) was considered to be 100%, and individual values were calculated as % of change. Data presented show the mean ± SD for each sample. Statistical analysis included Student's t test and one-way ANOVA, including all pairwise multiple comparison procedures (Holm-Sidak method).

(J–L) Summarized self-renewal data of n = 4 Ax-2 samples (J), n = 3 Ax-3 (K), and n = 2 Ax-4 (L) $CD34^+$ cells. Basal colony formation of original naive untreated cells pre-flight (H; Ax-2 L−45 days; I; Ax-3 L−30 days) was considered to be 100%, and individual values were calculated as % of change. Data presented show the mean ± SD for each sample. Statistical analysis included Student's t test and one-way ANOVA, including all pairwise multiple comparison procedures (Holm-Sidak method). p values less than 0.05 were considered significant.

Please cite this article in press as: Pham et al., Space-associated stem cell hallmarks of aging and resilience in astronauts, Cell Stem Cell (2025), https://doi.org/10.1016/j.stem.2025.11.001

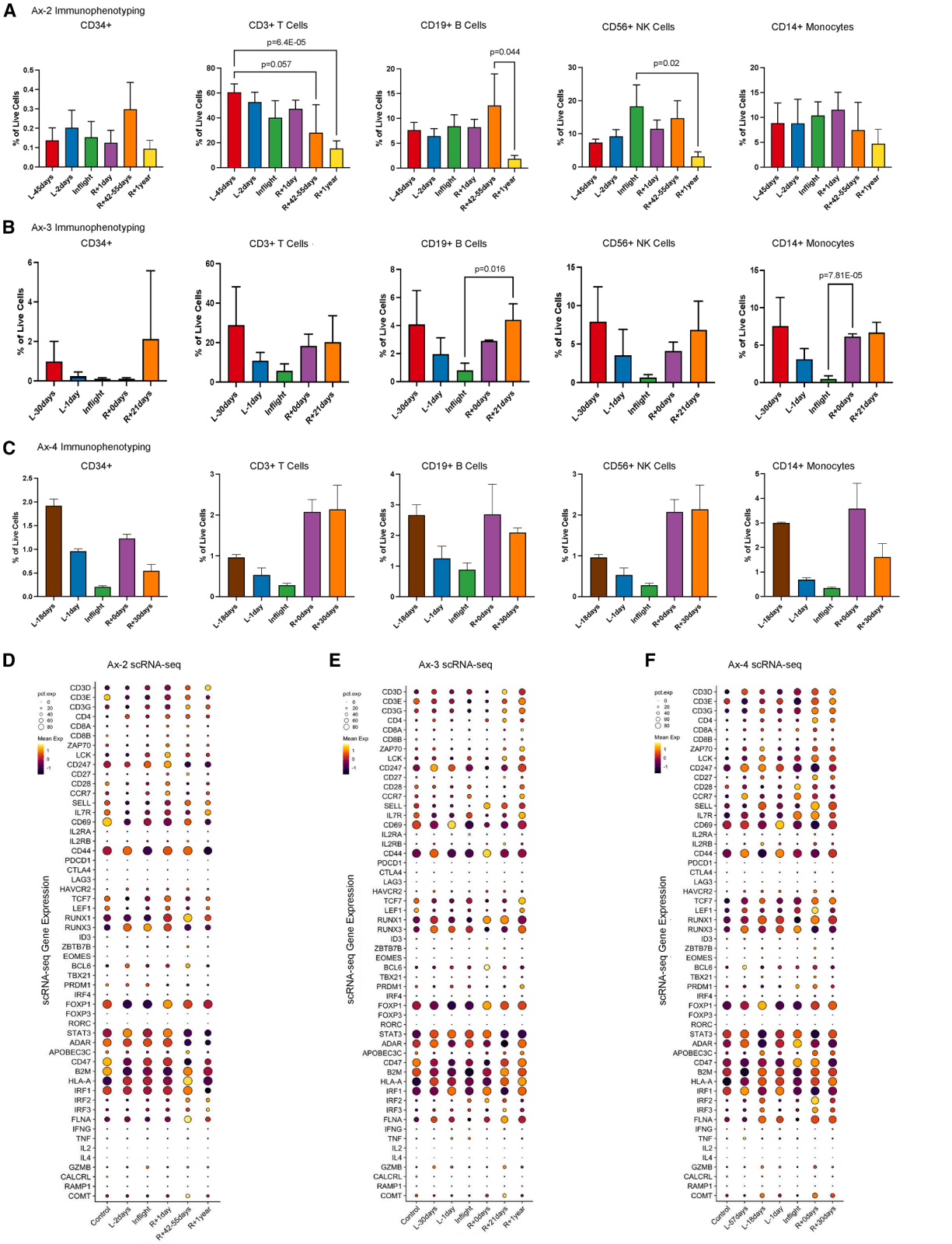

Figure 2. Space-associated immune repertoire alterations

(A–C) Immunophenotyping by FACS analysis of CD34$^+$ cells (CD3$^-$CD19$^-$CD56$^-$CD14$^-$), CD3$^+$ T cells, CD19$^+$ B cells, CD56$^+$ NK cells, and CD14$^+$ monocytes from bulk PBMCs isolated from Ax-2 (A), Ax-3 (B), and Ax-4 (C) astronauts. The Ax-2 mission includes time points up to R+42–55 days analyzed from

(legend continued on next page)

Please cite this article in press as: Pham et al., Space-associated stem cell hallmarks of aging and resilience in astronauts, Cell Stem Cell (2025), https://doi.org/10.1016/j.stem.2025.11.001

spaceflight (Figures 1B, 1C, S1G, and S1H). Specifically, scRNA-seq revealed differences in $CD34^{low}ADAR1^{high}$, $CD34^{+}CD38^{-}$, $CD34^{+}CD38^{mid}$, and $CD34^{+}CD38^{+}$ HSPC subpopulations inflight and immediately upon return in Ax-3 compared with Ax-2 crew members (Figures 1B and 1C). Within the $CD34^{+}$ population, particularly Ax-3 (21 days) and Ax-4 (20 days) crew members, we observed a transient population of cells with lower CD34 and higher expression of ADAR1, which has been linked to increased self-renewal capacity in HSPCs (Figures 1B and 1C).[28] Furthermore, scRNA-seq analysis of $CD34^{+}$ cells revealed alterations in G1 and S phases of the cell cycle during spaceflight in Ax-2 and Ax-3 missions (Figures 1D and 1E). Notably, scRNA-seq revealed a significant reduction in G1 and increase in S phase gene expression inflight from 21-day Ax-3 mission samples, suggesting that spaceflight duration may reduce HSPC dormancy, which has been linked to loss of self-renewal potential.[29–32]

To evaluate spaceflight-associated alterations in HSPC self-renewal and survival, fresh $CD34^{+}$ HSPCs were subjected to clonogenic survival and replating assays before, during, and after return from spaceflight. Long-term follow-up analyses were conducted to examine functional resilience over time. In keeping with spaceflight-associated stem cell aging, samples from Ax-2 and Ax-3 had significantly reduced multi-lineage colony formation inflight compared with all pre- and post-flight time points (Figures 1F, 1G, S1C, and S1E). HSPCs from Ax-4 ($n = 2$) samples followed a similar trend in multi-lineage colony formation reduction inflight compared with baseline, L−57 days (Figure 1I). While HSPC replating was similar to pre-flight in Ax-2 samples, there was a significant reduction in-flight compared with L−30 days in Ax-3 HSPC samples (Figures 1J, 1K, and S1D). A similar trend was observed in Ax-4 $CD34^{+}$ HSPC reduction in self-renewal capacity inflight compared with pre-flight, L−57 days (Figure 1L). Overall, astronaut HSPC self-renewal capacity after 21 days of time spent in low Earth orbit (LEO) was significantly reduced (Figure 1K) compared with L−45 days (Figure 1H). Notably, HSPCs derived from Ax-2 mission astronauts showed significantly increased self-renewal capacity immediately upon return (R+1 day) compared with pre-mission time points and remained elevated at R+1 year compared with baseline pre-flight samples (Figures 1J and S1D). Compared with Ax-2 samples, Ax-3 samples showed a significant reduction in self-renewal capacity in-flight as well as upon immediate return from LEO but rebounded to similar replating levels as Ax-2 samples 30 days after return to Earth (Figure S1F). Overall, these data underscore the functional impact of spaceflight duration on stem and progenitor cell repertoires.

Space-associated immune repertoire alterations

The landmark NASA Twins Study and SOMA studies have shown by multi-omics analyses that spaceflight induces immune alterations.[18,20] To characterize the impact of spaceflight duration on astronaut immune subpopulations, PBMCs from 49 samples were stained and analyzed by FACS. Ax-2 FACS analyses revealed a significant reduction in $CD3^{+}$ T cells (R+1 year) compared with pre-flight (L−45 days) (Figure 2A). Moreover, FACS analysis revealed persistent significant reductions of $CD19^{+}$ B cells and $CD56^{+}$ natural killer (NK) cells at R+1 year (Figure 2A). For Ax-3 crew members, FACS analysis showed reductions in $CD19^{+}$ B cells and $CD14^{+}$ monocytes inflight compared with pre-flight L−30 days and L−1 day, followed by a significant increase at R+0 and R+21 days (Figure 2B). Like Ax-3, Ax-4 crew members followed similar trends of reduction in $CD19^{+}$ B cells and $CD14^{+}$ monocytes inflight compared with pre-flight and an increase immediately upon return (Figure 2C). To further gauge the temporal sequence and depth of immune alterations, $CD4^{+}$ T cell subset FACS analyses of Ax-2 crew samples were performed and showed a slight reduction in $CD4^{+}$ central memory T cells at R+42–55 days compared with L−45 days, and similarly of $CD8^{+}$ naive T cells at R+42–55 days versus R+1 day (Figure S2A). Notably, parallel scRNA-seq analyses revealed a rebound by R+42–55 days and recovery to baseline at 1 year in most immune subsets following Ax-2 crew member return from space (Figure 2D). In Ax-3 crew member samples, FACS analyses revealed a trend toward reduced $CD4^{+}$ effector memory cells inflight compared with L−30 days (Figure S2B), and scRNA-seq analyses showed a commensurate reduction in T cell gene expression inflight (Figure 2E). Comparative scRNA-seq analyses of Ax-2 and Ax-3 samples revealed significant differences in interleukin (IL)-1β inflight, suggesting that inflammatory cytokine signaling deregulation may fuel immune repertoire differences (Figures S2C–S2H). Together, these data suggest that longer exposure to the LEO environment detrimentally impacts immune repertoires.

Space-associated HSPC telomere, mitochondrial, and cytokine deregulation

To assess the impact of spaceflight duration on HSPC inflammaging, we performed WGS analyses of telomere length and scRNA-seq analyses of telomere maintenance gene expression changes in nine astronauts, analyzing six time points for the Ax-2 mission, four for the Ax-3 mission, and five for the Ax-4 mission (Figures 3A–3C and S3A–S3C). As expected, considering the long length of telomeres in HSPCs compared with differentiated cells,[33,34] no significant telomere length changes were observed in the $CD34^{+}$ enriched HSPC fraction by WGS TelomereCat and TelSeq analyses (Figures 3A–3C and S3A–S3C). However, scRNA-seq analyses revealed significant space-associated reductions in both telomerase and CTC1-STN1-TEN1 polymerase α/primase (CST-POLA1) complex genes, which regulate telomere maintenance and also play a role in type 1 interferon activation (Figures 3D and S3D).[35,36] Compared with inflight, POLD2, a component of the CST-POLA1 telomere maintenance complex, and tripeptidyl peptidase 1 enzyme (TPP1), a shelterin protein that recruits telomerase to telomeres, remained

cryopreserved bulk PBMCs and fresh PBMCs at R+1 year. The Ax-3 mission includes time points up to R+21 days measured in fresh PBMCs. The Ax-4 mission includes time points L−18 days, L−1 day, inflight, R+0 days, and R+30 days measured in fresh PBMCs. Statistical significance was determined using a two-tailed *t* test of unequal variance for $n = 4$ Ax-4 and $n = 3$ Ax-3 samples. *p* values less than 0.05 were considered significant.
(D) Dot plot of T cell gene expression based on $CD3^{+}$ T cells from $n = 4$ Ax-2 (D), $n = 3$ Ax-3 (E), and $n = 2$ Ax-4 (F) scRNA-seq analysis. Statistical significance was determined by the Mann-Whitney U test with an false discovery rate (FDR) < 0.05.

Please cite this article in press as: Pham et al., Space-associated stem cell hallmarks of aging and resilience in astronauts, Cell Stem Cell (2025), https://doi.org/10.1016/j.stem.2025.11.001

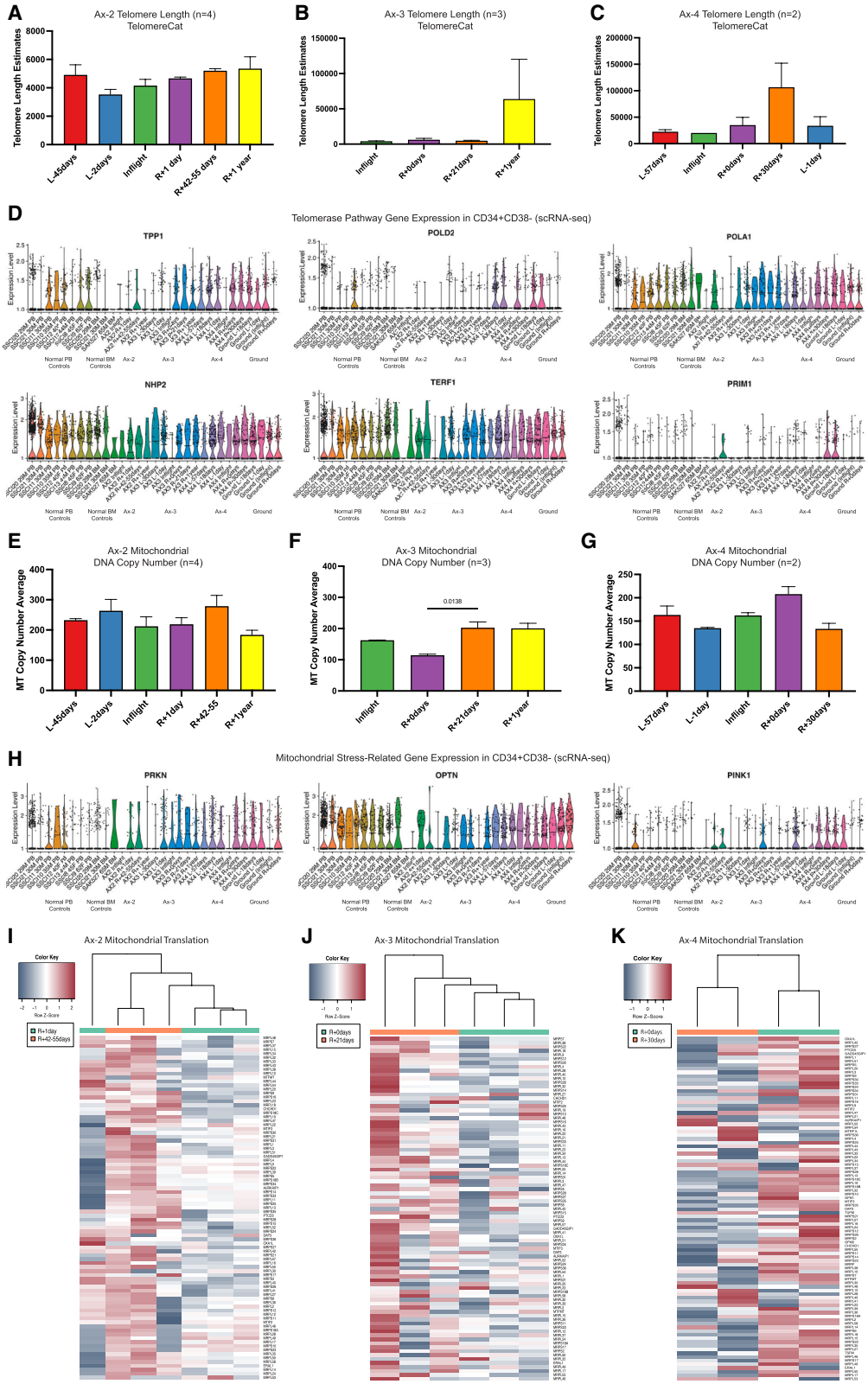

Figure 3. Space-associated HSPC telomere, mitochondrial, and inflammatory cytokine deregulation

(A–C) Bar graph illustrating WGS analysis of the average TelomereCat-estimated overall telomere length in base pairs (bp) of $CD34^+$ cells derived from Ax-2 (A), Ax-3 (B), and Ax-4 (C) samples. Ax-3 R+1 year time point includes $n = 2$ samples.

(legend continued on next page)

Please cite this article in press as: Pham et al., Space-associated stem cell hallmarks of aging and resilience in astronauts, Cell Stem Cell (2025), https://doi.org/10.1016/j.stem.2025.11.001

significantly reduced in CD34$^+$ HSPCs at R+1 year for Ax-2 crew members (Figure 3D). At R+21 days compared with inflight in the Ax-3 mission, CD34$^+$ cell scRNA-seq analyses showed a significant reduction in both DNA polymerase delta 2 (POLD2)-mediated telomere maintenance and the essential H/ACA ribonucleoprotein complex subunit 2 (NHP2) telomerase component, which has been associated with the accelerated aging syndrome dyskeratosis congenita when deregulated (Figures 3C and 3D).[37]

Regarding other key hallmarks of aging[15] and previous reports linking telomere length changes and mitochondrial DNA amplification,[18,38] mitochondrial DNA WGS analyses revealed significant mitochondrial DNA copy-number amplification in 21-day mission duration Ax-3 astronauts upon return in contrast to 10-day mission duration Ax-2 astronauts (Figures 3E, 3F, and S3C). Interestingly, we observed increased mitochondrial DNA amplification upon return that reflected both the significant increase in the S phase proportion of cells inflight and a cellular stress response (Figures 1D, 1E, 3H, and S3). In contrast to Ax-2 samples, GSEAs of pseudobulk data showed significant alterations in mitochondrial translation gene expression that distinguished R+0 days from R+21 days Ax-3 samples (Figures 3I, 3J, S3E, and S3F). For the mitochondrial translation genes in Ax-4, expression is (with the exception of the L−18 days samples) higher after return compared with pre-flight or inflight time points (Figure 3K). While there is a slight increase in expression for some genes in R+0 days (compared with R+30 days), the comparison of both Ax-3 and Ax-4 sets of post-flight time points to the inflight samples shows a substantial increase, which is indicative of sustained mitochondrial stress responses associated with longer mission duration.

Furthermore, SASHA-R research involved cytokine analysis of diluted plasma collected from 7 (Ax-2 and Ax-3 mission) astronauts across various time points, as well as RNA-seq analyses of cytokine gene and cytokine receptor expression from 3 Ax-3 time points (Figures S3G–S3J). These analyses demonstrated significantly increased levels of pro-inflammatory IL-23 expression inflight for both Ax-2 and Ax-3 crew members (Figures S3G and S3H). Interestingly, an increase in IL-23 was already apparent pre-flight (L−2 days) for Ax-2 astronauts. In contrast to Ax-2 crew members, Ax-3 crew members showed a significant increase in IL-10 and a decrease in IL-15 inflight (Figures S3G and S3H). Finally, RNA-seq analyses of cytokine and cytokine receptor expression measured at L−45 days, L−2 days, and inflight for Ax-2 HSPCs showed overall deregulation (Figures S3I and S3J), suggesting that hallmarks of HSPC inflammaging are acquired in response to stressors associated with spaceflight.

Dynamic space-associated clonal HSPC mutations

To determine the contribution of space radiation-induced somatic mutagenesis in HSPCs, we obtained NASA radiation logs from six locations on the ISS during these PAMs. Based on these NASA ISS dosimetry logs, we determined the average dose rate of exposure and human tissue dose equivalent during Ax-2 (May 22, 2023–May 30, 2023) and Ax-3 (January 20, 2024–February 7, 2024).[39] These measurements include Earth's magnetic field, galactic cosmic rays (GCRs), and solar particle events (SPEs) for which there were 0 events detected during both Axiom missions. Specifically, the human tissue dose equivalents of radiation were 0.460 and 0.521 mSv/day for Ax-2 and Ax-3, respectively (Figures 4A and S1B). Interestingly, MutationalPatterns analyses showed that only a minority of C>T mutations were located in CpG dinucleotide sites, thereby suggesting that ionizing radiation was not the only contributor to mutagenesis and that WGS analyses would need to be employed sequentially to resolve space-specific mutagenesis patterns[40] (Figure S4A).

To determine if HSPC mutations were acquired during spaceflight in Ax-2, CD34$^+$ enriched cells were subjected to 90× WGS at L−2 days, inflight, R+1 day, R+42–55 days, and R+1 year. Results were compared with pre-flight L−45 days (Figures 4B–4D). A similar analysis was completed for Ax-3, with return time points at R+0 days and R+21 days and results normalized to inflight (Figures 4F–4I). For Ax-4, WGS analysis included L−1 day, inflight, R+0 days, and R+30 days normalized to L−57 days (Figures 4J–4M). While most somatic mutations acquired across the study (Figures 4E, 4I, 4M, and S4B–S4G) were C-to-T single base substitutions (SBSs) with a few double base substitutions (DBSs), a significant increase in insertions and deletions (indels) was detected at R+21 days compared with R+0 days in Ax-3 crew members (Figure 4H).

Regarding space-associated clonal hematopoiesis (CH) (SACH), single-sample mode analysis was performed with a cut-off of 10% variant allele frequency (VAF) and revealed that one Ax-2 astronaut had a pre-launch clonal cAMP-response element binding protein (CREBBP) mutation (Figure 4Q). Three of the four astronauts had detectable CH mutations at R+1 year, including KDM6A, NOTCH3, CSF3R, and SMC1A. In contrast to Ax-2, we observed increased acquisition of CH-associated mutations inflight for the 21-day mission duration of the Ax-3 crew

(D) Violin plots of mitochondrial stress-related gene expression in CD34$^+$CD38$^-$ cells from normal control samples derived from normal age-matched peripheral blood, young and aged bone marrow, and Ax-2 and Ax-3 astronauts. SSCI 8–21 are normal age-matched donor PBMCs or SAK527 and SAK528 derived from normal-aged bone marrow (BM). Telomerase pathway genes include TPP1, POLD2, POLA1, NHP2, TERF1, and PRIM1.

(E–G) Bar graph of average mitochondrial copy-number estimates (*y* axis) from Ax-2 (E), Ax-3 (F), and Ax-4 (G) samples over time (*x* axis) measured by WGS. Ax-2 time points include $n = 4$ L−45 days, L−2 days, inflight, R+1 day, R+42–55 days, and R+1 year. Ax-3 time points include $n = 3$ inflight, R+0 days, R+21 days, and R+1 year ($n = 2$). Ax-4 time points include $n = 2$ L−57 days, L−1 day, inflight, R+0 days, and R+30 days. Statistical significance was determined by a two-way ANOVA with Tukey's multiple comparisons test. p values less than 0.05 were considered significant.

(H) Violin plots of mitochondrial stress-related gene expression in CD34$^+$CD38$^-$ cells from normal control samples derived from normal age-matched peripheral blood, young and aged bone marrow, and Ax-2 and Ax-3 astronauts. SSCI 8–21 are normal age-matched donor PBMCs or SAK527 and SAK528 derived from normal-aged BM. Telomerase pathway genes include PRKN, OPTN, and PINK1.

(I–K) For the sample groups R+1 day and R+42–55 days from Ax-2 (I), R+0 days and R+21 days from Ax-3 (J), and R+0 days and R+30 days from Ax-4 (K), pseudobulk counts were used to generate a heatmap for the expressed genes in the mitochondrial translation category. In the GSEA for Ax-2 (I), this category had a nominal $p < 0.005$, and the majority of genes had a positive logFC, indicating expression greater in the R+42–55 days group. In the GSEA for Ax-3 (J), this category had an adjusted $p < 0.05$, and the majority of genes had a positive logFC, indicating expression greater in the R+21 days group. In the GSEA for Ax-4 (K), this category had an adjusted $p < 0.05$, and the majority of genes had a positive logFC, indicating expression greater in R+0 days group.

Please cite this article in press as: Pham et al., Space-associated stem cell hallmarks of aging and resilience in astronauts, Cell Stem Cell (2025), https://doi.org/10.1016/j.stem.2025.11.001

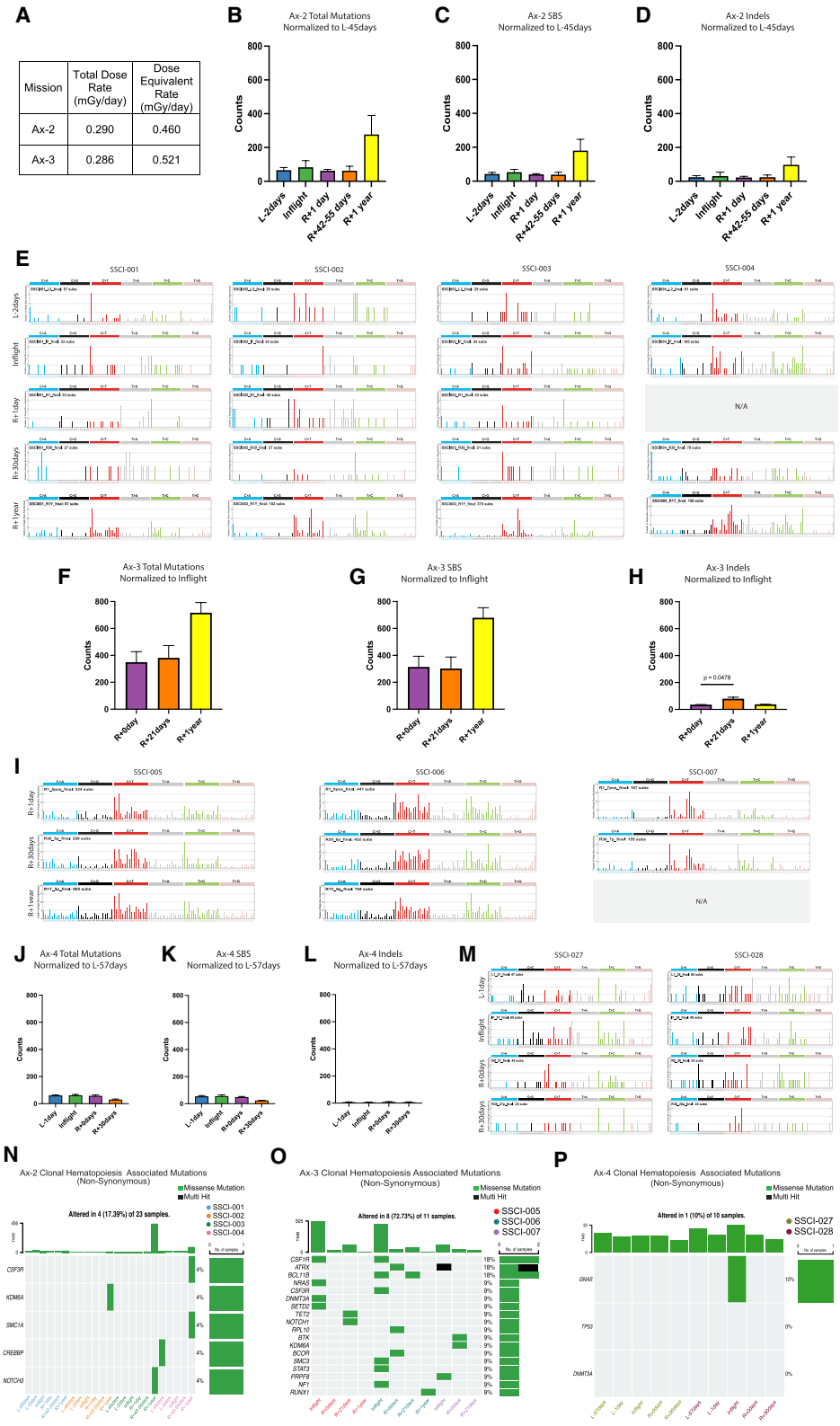

Figure 4. Dynamic space-associated somatic mutations and clonal HSPC mutations

(A) Total radiation averaged from seven locations on the ISS for the duration of the Ax-2 and Ax-3 missions. Average radiation based on GCRs, trapped particles (South Atlantic anomaly), and solar particles (extreme solar particle events).

(legend continued on next page)

Please cite this article in press as: Pham et al., Space-associated stem cell hallmarks of aging and resilience in astronauts, Cell Stem Cell (2025), https://doi.org/10.1016/j.stem.2025.11.001

(Figure 4R). Notably, one astronaut acquired a mutation in BCL11B inflight, which reappeared at R+21 days. Like Ax-2, one Ax-3 astronaut acquired a mutation in RUNX1, a transcription factor important for regulating HSC self-renewal, at R+1 year, thereby underscoring the importance of yearly CH analyses for astronauts. One of two Ax-4 astronauts acquired a missense mutation in guanine nucleotide-binding protein alpha stimulating activity polypeptide 1 (GNAS) during spaceflight, which was no longer detectable upon return (Figure 5P). Additional single base substitutions acquired in response to spaceflight were observed and suggestive of APOBEC3C base deaminase activation (Figures S4Q–S4S).[26] Notably, the observed increase in CH-associated mutations in Ax-3 suggests that the longer-duration missions may impact human HSPC fitness and predispose to pre-cancer stem cell generation[13] in a spaceflight duration-dependent manner. Despite an increase in CH mutations following spaceflight, the majority of CH mutations were no longer detectable at R+1 year, underscoring the dynamic nature of CH and revealing possible HSPC resilience mechanisms in response to stress.

Space-associated ADAR1 and APOBEC3C base deaminase deregulation

Both ADAR1 and APOBEC3C base deaminase deregulation have been linked to pre-cancer stem cell propagation and cancer stem cell generation in inflammatory microenvironments, particularly in myeloproliferative neoplasms (MPNs)[13,28,41,42] and acute myeloid leukemia (AML)[43] and thus were studied in Ax-2, Ax-3, and Ax-4 astronaut crew members before, during, and after spaceflight to ascertain their respective roles in SACH (Figures 5A–5K).[1,5,44,45] While scRNA-seq revealed that ADAR1 expression increased during spaceflight in CD34$^+$ cells in Ax-3 more than Ax-2 missions (Figures 5A–5F), corresponding with the observed increased G1 to S phase transition in Ax-3 (Figures 1D and 1E), post-spaceflight analyses revealed a significant reduction in ADAR1 base deaminase expression levels in both Ax-2 and Ax-3 crew members (Figures 5G, 5H, S5C, and S5D). A similar reduction in ADAR1 expression was observed in Ax-4 HSPC ADAR1 expression levels upon return (Figure 5I). This decline corresponds with the observed diminished replating capacity (Figures 1J–1L), consistent with ADAR1's well-established role in regulating HSC self-renewal.[28] Furthermore, within HSPCs, we detected increased protein C receptor (PROCR) expression, the gene that encodes the endothelial protein C receptor (EPCR), which is a marker of a highly regenerative stem cell population, suggesting enhanced regenerative self-renewal capacity upon return (Figures 1J–1L and 5D–5F). To further investigate the role of ADAR1-mediated RNA editing in HSPC functional decline following spaceflight, pseudobulk RNA editing (editome) analysis revealed a transient missense editing event in

(B) Bar plot showing the total amount of somatic mutations (SBS and indels) from CD34$^+$ cells acquired across the study time points in Ax-2, including L−2 days, inflight, R+1 day, R+42–55 days, and R+1 year. The data from each time point are normalized to L−45 days. No significant differences between time points by two-way ANOVA with Tukey's multiple comparisons test.
(C) Bar plot showing the total number of somatic SBSs from CD34$^+$ cells acquired across the study time points in Ax-2, including L−2 days, inflight, R+1 day, R+42–55 days, and R+1 year. The data from each time point are normalized to L−45 days. No significant differences between time points by two-way ANOVA with Tukey's multiple comparisons test.
(D) Bar plot showing the total number of somatic indels from CD34$^+$ cells acquired across the study time points in Ax-2, including L−2 days, inflight, R+1 day, R+42–55 days, and R+1 year. The data from each time point are normalized to L−45 days. No significant differences between time points by two-way ANOVA with Tukey's multiple comparisons test.
(E) Patterns of SBS for the Ax-2 samples are shown using the SBS96 classification scheme on the *x* axis. The *y* axis is scaled differently in each plot to optimally show each mutational pattern, with the *y* axis reflecting the number of mutations for the respective mutational scheme. The data from each time point are normalized to L−45 days. Sample SSCI-004 at R+1 day could not be collected for WGS.
(F) Bar plot showing the total amount of somatic mutations (SBS and indels) from CD34$^+$ cells acquired across the study time points in Ax-3, including R+0 days, R+21 days, and R+1 year. The data from each time point are normalized to inflight. R+0 days and R+21 days include $N = 3$ samples, and R+1 year time point includes $n = 2$ samples. No significant differences between time points by two-way ANOVA with Tukey's multiple comparisons test.
(G) Bar plot showing the total number of somatic SBSs from CD34$^+$ cells acquired across the study time points in Ax-3, including R+0 days, R+21 days, and R+1 year. The data from each time point are normalized to inflight. R+0 days and R+21 days include $N = 3$ samples, and R+1 year time point includes $n = 2$ samples. No significant differences between time points by two-way ANOVA with Tukey's multiple comparisons test.
(H) Bar plot showing the total number of somatic indels from CD34+ cells acquired across the study time points in Ax-3, including R+0 days, R+21 days, and R+1 year. The data from each time point are normalized to inflight. R+0 days and R+21 days include $N = 3$ samples, and R+1 year time point includes $n = 2$ samples. Statistical analysis was determined by two-way ANOVA with Tukey's multiple comparisons test. *p* values less than 0.05 were considered significant.
(I) Patterns of SBS for the Ax-3 samples are shown using the SBS96 classification scheme on the *x* axis. The *y* axis is scaled differently in each plot to optimally show each mutational pattern, with the *y* axis reflecting the number of mutations for the respective mutational scheme. The data from each time point are normalized to inflight. Sample SSCI-007 at R+1 year could not be collected.
(J) Bar plot showing the total amount of somatic mutations (SBS and indels) from CD34$^+$ cells acquired across the study time points in Ax-4, including L−1 day, inflight, R+0 days, and R+30 days. The data from each time point are normalized to L−57 days. No significant differences between time points by two-way ANOVA with Tukey's multiple comparisons test.
(K) Bar plot showing the total number of somatic SBSs from CD34$^+$ cells acquired across the study time points in Ax-4, including L−1 day, inflight, R+0 days, and R+30 days. The data from each time point are normalized to L−57 days. No significant differences between time points by two-way ANOVA with Tukey's multiple comparisons test.
(L) Bar plot showing the total number of somatic indels from CD34$^+$ cells acquired across the study time points in Ax-4, including L−1 day, inflight, R+0 days, and R+30 days. The data from each time point are normalized to L−57 days.
(M) Patterns of SBS for the Ax-4 samples are shown using the SBS96 classification scheme on the *x* axis. The *y* axis is scaled differently in each plot to optimally show each mutational pattern, with the *y* axis reflecting the number of mutations for the respective mutational scheme. The data from each time point are normalized to L−57 days.
(N) Oncoplot displaying CH mutated genes acquired in CD34$^+$ cells from each individual per time point of Ax-2 (N), Ax-3 (O), and Ax-4 (P) missions. Samples SSCI-004 at R+1 day and SSCI-007 at R+1 year could not be collected.

Please cite this article in press as: Pham et al., Space-associated stem cell hallmarks of aging and resilience in astronauts, Cell Stem Cell (2025), https://doi.org/10.1016/j.stem.2025.11.001

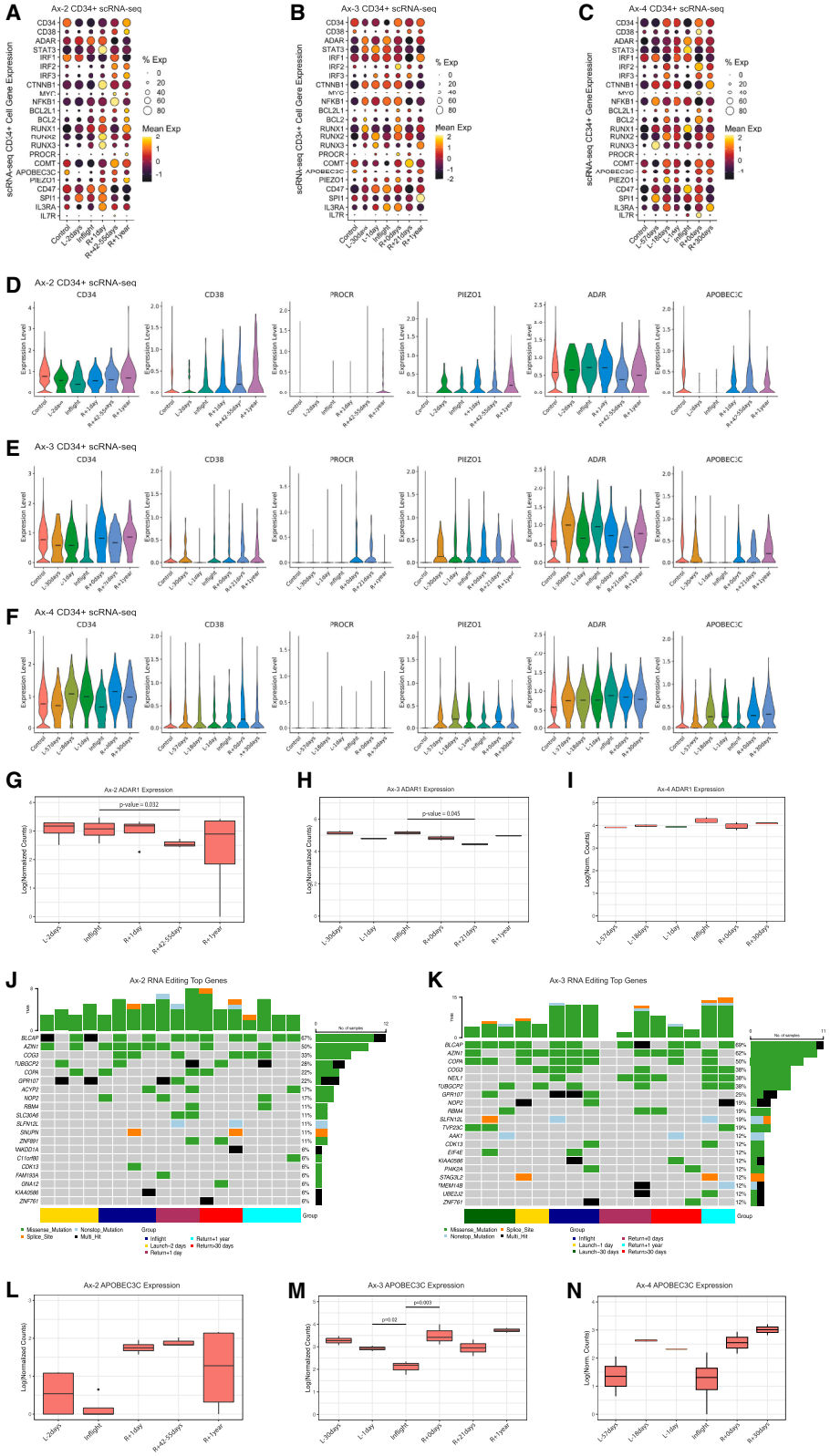

(legend on next page)

Please cite this article in press as: Pham et al., Space-associated stem cell hallmarks of aging and resilience in astronauts, Cell Stem Cell (2025), https://doi.org/10.1016/j.stem.2025.11.001

cyclin-dependent kinase 13 (CDK13), a splicing and cell cycle regulatory gene previously found to be edited in MPNs (Figures 5J and 5K).[13] Moreover, antizyme inhibitor 1 (AZIN1), a well-known target of ADAR1 editing, was found to be edited in-flight during both space missions corresponding with ADAR1 activation during spaceflight (Figures 5J and 5K). Interestingly, while only one astronaut presented with an AZIN1 missense edit before spaceflight, multiple astronauts exhibited a missense edit in AZIN1 pre-flight, inflight, or post-flight (Figures 5J and 5K). Finally, scRNA-seq pseudobulk analyses revealed significant upregulation of base deaminase APOBEC3C upon return from spaceflight (Figures 5L–5N and S5E–S5G), indicative of a base deaminase-mediated mechanism of C-to-T mutagenesis in response to spaceflight that may fuel SACH.

Space-associated retrotransposon deregulation

Both primate-specific APOBEC3 and ADAR1 deaminases evolved to protect long-lived human stem cell populations from retroviral integration and genomic instability related to retrotransposon activation, including long interspersed nuclear elements (LINEs), Alu's, and human endogenous retroviruses (HERVs).[12,46,47] Previously, we observed that LINE deregulation in post-spaceflight compared with ground HSPC niche nanobioreactors was associated with functional HSPC aging. Therefore, we analyzed retrotransposon expression utilizing RNA-seq available for Ax-2 mission time points (n = 2 L−30 days, n = 4 L−2 days, and n = 2 inflight). In these analyses, we observed that retrotransposon expression changes occurred pre-flight as part of a possible fight or flight response and became more pronounced during spaceflight, with unsupervised hierarchical clustering clearly distinguishing the analyzed time points, specifically LINEs and HERVs (Figures 6A and S6A–S6D). Furthermore, LINE-1-specific analyses revealed a significant reduction of LIME3A upon exposure to microgravity, which interestingly was already downregulated at L−2 days compared with L−45 days (Figures S6A and S6B).

To assess the regulation of retrotransposons in response to aging and LEO exposure, we performed scTE analyses on young, middle-aged, and older peripheral blood and bone-marrow-derived HSPCs and compared these analyses with Ax-2, Ax-3, and Ax-4 crew member HSPCs before, during, and after spaceflight (Figures 6B–6E). These scRNA-seq analyses showed that LINEs were significantly upregulated upon return from the Ax-2 mission and continued to be highly expressed at R+1 year in a manner similar to aged HSPC samples (Figure 6C). The LINEs were highly expressed inflight and at R+0 days for the Ax-3 crew but returned to pre-flight levels by R+21 days (Figures 6B and S6E). A temporal association between ADAR1 upregulation and LINE overexpression was more prominent in Ax-3 compared with Ax-2 crew members by scRNA-seq TE analyses, suggesting a regulatory role of ADAR1. Interestingly, HERVs were highly expressed at R+1 year in Ax-2 (Figures 6D and S6F). Similarly, ADAR1 expression increased during spaceflight in Ax-3 crew members commensurate with HERV upregulation (Figure 6D). Perhaps equally importantly, specific HERVs were activated in Ax-2, Ax-3, and Ax-4 HSCs in response to spaceflight, and overall HERV expression varied in an astronaut-dependent manner (Figures 6D and 6E).

In addition to changes in retrotransposon activation, return to Earth was associated with increased expression of the mechanoreceptor gene, PIEZO1, as well as expression of nociceptive and fight or flight response genes, including receptor activity modifying protein 1 (RAMP1), calcitonin receptor-like receptor (CALCRL), and catechol-O-methyltransferase (COMT) in Ax-2, Ax-3, and Ax-4 HSPCs (Figures 6B and 6D).[8,48] Remarkably, calcium/calmodulin-dependent protein kinase II alpha (CAMK2A), a gene central to the fight or flight response in response to stress,[49] was significantly changed inflight with the greatest $\log_2$ fold change ($\log_2$FC) in Ax-3 and Ax-4 (Figures 6B, 6D, S2D, and S2E). Together, these human-specific retrotransposon and fight or flight response gene expression alterations provide valuable insights into drivers of accelerated aging under conditions of extreme stress and warrant long-term evaluation of the impact of spaceflight on HSPC fitness as well as targeted countermeasure development to enable future missions.

DISCUSSION

Seminal research shows that spaceflight induces immune dysregulation,[18,19,22–25] physiologic changes, and sustained molecular and cellular changes in tissues. However, these effects were not directly studied in purified HSPC populations, which give rise to immune subpopulations that protect from latent virus reactivation and pre-cancer evolution to cancer.[1] In this SASHA-R study in astronauts, our aim was to understand how spaceflight duration impacts HSPC functional resilience and contributes to immune system deregulation before, during, and after space missions. Using 51 fresh blood specimens collected sequentially from 9 astronauts during the Ax-2 10-day, Ax-3 21-day, and Ax-4 20-day missions to the ISS, we profiled 4,694 HSPCs and 312,585 total cells and investigated the functional and molecular characteristics of HSPCs in the context of hallmarks of aging[15] by integrating scRNA-seq with HSPC-FOMA-R-focused functional analyses and whole-genome and

Figure 5. Space-associated ADAR1 and APOBEC3C base deaminase deregulation

(A–C) Dot plot of HSC gene expression based on CD34$^+$ cells from Ax-2 (A), Ax-3 (B), and Ax-4 (C) scRNA-seq analysis.

(D–F) Violin plots showing key gene expression based on CD34$^+$ cells from Ax-2 (D), Ax-3 (E), and Ax-4 (F) by scRNA-seq analysis. Genes include CD34, CD38, PROCR, PIEZO1, ADAR, and APOBEC3C. Statistics were determined by the Mann-Whitney U test with an FDR < 0.05.

(G–I) Log expression of ADAR1 in pseudobulk generated counts from scRNA-seq of CD34-positive cells derived from the peripheral blood of individuals at time points before, during, or after time spent in LEO. Data from the Ax-2 mission (G), the Ax-3 mission (H), and the Ax-4 mission (I). Statistics were determined by Student's t test assuming equal variance. p values less than 0.05 were considered significant. No significant differences between adjacent time points.

(J and K) Oncoplot visualization shows the top 20 edited genes across all time points in Ax-2 (J) and Ax-3 (K). The bar graph across the top shows total editing events in each sample for the top 20 genes, while bar graph on the right edge shows the percentage of samples with edits in the gene.

(L–N) Log expression of APOBEC3C in pseudobulk generated counts from scRNA-seq of CD34-positive cells derived from the peripheral blood of individuals at time points before, during, or after time spent in LEO. Data from the Ax-2 mission (L), the Ax-3 mission (M), and the Ax-4 mission (N). Statistics were determined by Student's t test assuming equal variance. p values less than 0.05 were considered significant.

Please cite this article in press as: Pham et al., Space-associated stem cell hallmarks of aging and resilience in astronauts, Cell Stem Cell (2025), https://doi.org/10.1016/j.stem.2025.11.001

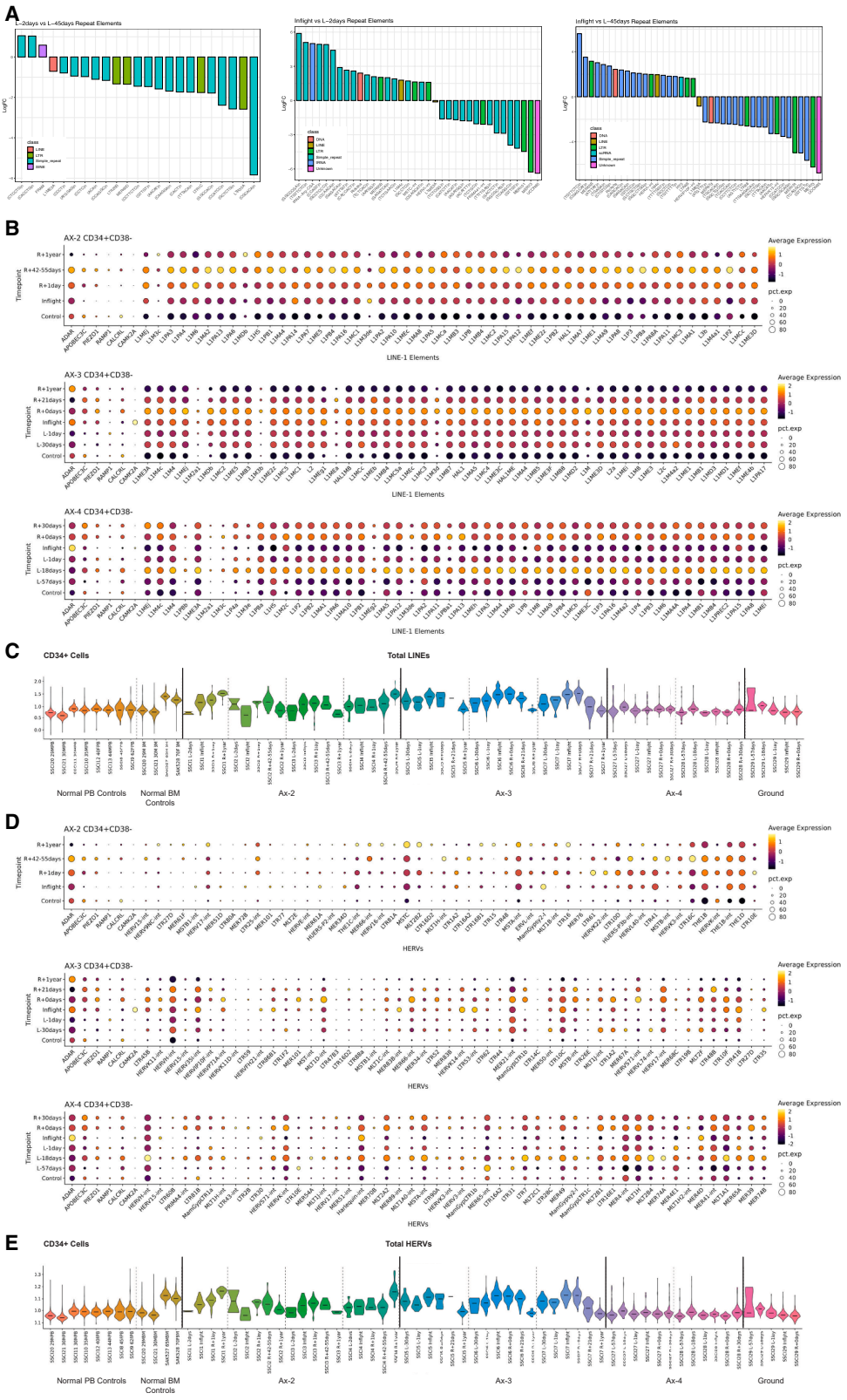

(legend on next page)

Please cite this article in press as: Pham et al., Space-associated stem cell hallmarks of aging and resilience in astronauts, Cell Stem Cell (2025), https://doi.org/10.1016/j.stem.2025.11.001

transcriptome sequencing to assess HSPC clonogenicity and self-renewal capacity, evaluate mutational burden, identify mutational signatures, and enhance transcript coverage for retrotransposon analyses. We observed decreased HSPC self-renewal, reduced ADAR1 expression and editing levels, elevated APOBEC3C expression, space-induced DNA mutagenesis, and dynamic retrotransposon changes.

While pioneering NASA studies in astronauts detected inflammatory cytokine changes, mitochondrial DNA amplification, and telomere length changes,[18,19,21,24,25,50–52] these analyses focused on short-lived PBMCs[53,54] rather than the long-lived HSPC compartment.[18] Thus, we sought to understand the cumulative functional and molecular impact of variable duration (10 days, 21 days, versus 20 days) exposure to the LEO environment (microgravity and chronic radiation) on HSPCs. As expected, based on the long telomere length of HSPCs, telomere length was not significantly altered in $CD34^+$ cells. However, the CST-POLA1 complex and telomere maintenance genes were significantly changed, as shown by scRNA-seq. Specifically, POLD2, a telomere maintenance gene, and TPP1, which recruits telomerase to telomeres, were significantly and persistently downregulated following a mission duration of 10 days in Ax-2 crew members. Moreover, Ax-3 (21-day mission) crew members also harbored a persistent decrease in POLD2 as well as significantly decreased expression of the telomerase gene, NHP2, which is a vital component of the telomerase complex and can lead to telomere shortening and premature aging when deregulated.[37] These data suggest that longer mission duration has a more profound impact on both the telomerase complex and telomere maintenance genes.

Despite the observed variability among astronauts, these findings, along with indications of stem cell exhaustion based on HSPC-FOMA-R-focused scRNA-seq-based cell cycle assessments and self-renewal assays, support the observations that spaceflight accelerates HSPC aging. Our WGS, RNA-seq, and scRNA-seq data suggest that HSPC population dynamics contribute to telomere maintenance changes during spaceflight with the emergence of a highly regenerative PROCR- and ADAR1-high HSPC population that coincides with upregulation of both LINEs and HERVs retrotransposon expression.

The self-renewal potential of HSCs is regulated, in part, by ADAR1 activity.[41] A decrease in ADAR1 expression may be linked to the significantly reduced self-renewal capacity observed throughout different time points of the missions. Additionally, reduced ADAR1 expression also poses a risk for the reactivation of latent viruses[55] and the derepression of retrotransposons.[56] Specifically, upregulation of LINE and HERV expression closely aligned with increased ADAR1 expression. Although these changes appear to be transient and the human body demonstrates resilience, differences between the Ax-2, Ax-3, and Ax-4 missions suggest that time in space is a significant contributor to genomic instability and inflammaging through retrotransposon deregulation.

Our results suggest that HSPC-FOMA-R changes associated with launch occur in a spaceflight duration-dependent manner. In addition to the duration-dependent effects seen during and after spaceflight in the two longer missions, we noticed a pre-flight HSPC-FOMA-R response immediately before launch (Ax-2 L−2 days, Ax-3 L−1 day, and Ax-4 L−18 days and L−1 day). Pre-flight data suggest a fight or flight associated response, characterized by modulation of RAMP1, linked to nociceptive nerve regulation of HSC mobilization.[8] Notably, Ax-4 astronauts had an unexpected launch delay with an additional pre-flight sample drawn at L−18 days that demonstrated activation of an HSPC fight or flight response, typified by increased expression of CALCRL, COMT, and RAMP1, as well as LINEs and HERVs retrotransposon derepression. Interestingly, significantly differentially expressed CAMK2A in Ax-3 and Ax-4 suggests that another fight or flight response occurred inflight immediately prior to hatch closure and return to Earth. Notably, changes in inflammatory cytokine levels, cell cycle dynamics, and retrotransposon expression were already observed pre-flight, which might coincide with the fight or flight response seen in bone marrow under conditions of extreme stress.[8,57] Hematopoietic stress has also been suggested to trigger retrotransposon transcription in HSCs, causing HSCs to move out of their quiescent state.[47] Further, the differentiation of HSPCs to immune cells may be regulated by activation of retrotransposons, such as endogenous retroviruses, so repression or changes in retrotransposon expression may have a negative effect on the immune response.[46] Changes to the innate immune response may trigger type 1 interferon, which has been linked to ADAR1 activation and has been shown to regulate retrotransposons after tissue injury.[13,47]

As the first comprehensive study of stem cell health in astronauts, our HSPC-FOMA-R study revealed nine significant hallmarks of accelerated aging in a time-in-space-dependent manner, including (1) loss of dormancy, (2) reduced self-renewal commensurate with reduced ADAR1 self-renewal gene

Figure 6. Space-associated retrotransposon deregulation

(A) Waterfall plots of the expression of the top 40 significant repeat elements (and L1ME3A) in each comparison of time points (L−2 days versus L−45 days, left; inflight versus L−2 days, center; inflight versus L−45 days, right). The *y* axis represents the log-fold change for the comparison, while the *x* axis indicates the repeat element, with the bar colored by the family of the repeat.

(B) Dot plots generated from scTE analysis of LINEs expression of $CD34^+CD38^-$ cells from Ax-2, Ax-3, and Ax-4. The top 50 significantly differentially expressed (adj. $p < 0.05$) retrotransposons with the highest absolute log-fold change at any time point and control $CD34^+CD38^-$ HSCs from healthy donor PBMCs.

(C) Violin plot of the LINEs' total expression scores generated with AddModuleScore in all $CD34^+$ HSPCs for each individual astronaut across time points and normal control samples derived from peripheral blood and bone marrow $CD34^+$ HSPCs. SSCI 8–21 are normal age-matched donor PBMCs or SAK527 and SAK528 derived from normal-aged BM.

(D) Dot plots generated from scTE analysis of HERVs expression of $CD34^+CD38^-$ cells from Ax-2, Ax-3, and Ax-4. The top 50 significantly differentially expressed (adj. $p < 0.05$) retrotransposons with the highest absolute log-fold change at any time point and control $CD34^+CD38^-$ HSCs from healthy donor PBMCs.

(E) Violin plot of HERV total expression scores generated with AddModuleScore in all $CD34^+$ HSPCs for each individual astronaut across time points and normal control samples derived from peripheral blood and bone marrow $CD34^+$ HSPCs. SSCI 8–21 are normal age-matched donor PBMCs or SAK527 and SAK528 derived from normal-aged BM.

Please cite this article in press as: Pham et al., Space-associated stem cell hallmarks of aging and resilience in astronauts, Cell Stem Cell (2025), https://doi.org/10.1016/j.stem.2025.11.001

expression, (3) reduced multi-lineage colony formation, (4) reduced telomere maintenance, (5) increased mitochondrial copy number and mitochondrial stress-related gene expression, (6) genomic instability typified by increased indels, (7) SACH, (8) APOBEC3C base deaminases deregulation, and (9) cell-type and context-specific HERV and LINE retrotransposon activation.[1,15] While these hallmarks were observed in three independent PAMs, we detected a transient population of cells with higher expression of PROCR, suggesting a level of functional resilience to SASHA. Overall, these results enable prediction of HSPC-FOMA-R and ultimately inform the development of prevention strategies for accelerated stem cell aging in response to stress, including in spaceflight.

Limitations of the study

This study focuses on the temporal sequence of space-associated HSPC aging in three separate PAMs to the ISS to demonstrate the acquisition of CH mutations, alterations in telomere maintenance and inflammatory cytokines, and deregulation of base deaminases and retrotransposons over time. As an active long-term study, yearly follow-up has not been concluded for all astronauts, and results are pending to determine whether current changes observed have prolonged effects on stem cell fitness. Due to the paucity of $CD34^+$ HSPCs in peripheral blood, cell availability limited the number of downstream assays possible, although we were able to study many functional and molecular hallmarks of stem cell aging.[15,16] Combined with shifting launch and private crew schedules, comparisons between the 10-, 21-, and 20-day missions were performed with as much standardization as possible. However, conclusions regarding the effects of spaceflight duration are based on this limited number of missions, and the possibility remains that random variation among flights or uncontrolled variables, independent of flight length, have contributed to differences in aging hallmarks and resilience observed in the Axiom 2 versus Axiom 3 and 4 missions. Additionally, due to the longitudinal nature of this study, there was some variability between reagent kits, specifically library preparation kits and sequencing platforms, depending on chemistry and instrument advancements and availabilities that should be taken into consideration. Despite these differences, we performed robust analyses with statistically significant results that provide unique tools for predicting accelerated HSPC aging in response to stress, including in response to spaceflight.

RESOURCE AVAILABILITY

Lead contact

Further information and requests for resources and reagents should be directed to and will be fulfilled by the lead contact, Catriona H.M. Jamieson (cjamieson@health.ucsd.edu).

Materials availability

This study did not generate new reagents.

Data and code availability

- Whole-transcriptome RNA-seq, scRNA-seq, and WGS data will be deposited at the database of Genotypes and Phenotypes (dbGaP) at NIH. Accession numbers are listed in the key resources table. Any additional information required to reanalyze the data reported in this paper is available from the lead contact upon request.
- All code and somatic mutation analysis methods are publicly available under the permissive 2-clause BSD license via the GitHub repository. Links are provided in the key resources table. All other computational tools utilized in this publication have been mentioned in the methodology section and can be accessed through their respective publications.

ACKNOWLEDGMENTS

We would like to acknowledge the significant contributions of the Axiom 2, Axiom 3, and Axiom 4 astronauts; Michelle Ortiguerra, MBA; and other members of the UC San Diego Sanford Stem Cell Institute (SSCI) and the Salk Institute NGS Core Facility. We are grateful to our funding agencies for their vital support, including NASA (NRA NNJ13ZBG001N), NCI (R01CA296974), NCI (R01CA205944), NIH/NIDDK (R01DK114468-01), NIH NCI CCSG p30CA023100, NIH NCI CCSG P30 CA01495, NIH NIA San Diego Nathan Shock Center (P30 AG068635), The Chapman Foundation and the Helmsley Charitable Trust, LLS Blood Cancer Discoveries, SSCI, the Koman Family Foundation, the JM Foundation, and the Moores Family Foundation.

AUTHOR CONTRIBUTIONS

C.H.M.J., J.P., L.B., and L.B.A. conceived the study. J.P., S.P.N., L.B., C.E., P.C., K.M., I.v.d.W., E.K., J. Sneifer, N.K., K.W., A.R., D.C.-F., E.M., J. Stoudemire, S.R.M., T.W., and L.B.A. designed and/or performed experiments and analyzed data. T.W. performed RNA-seq and RNA editing analyses and data deposition, supervised by C.H.M.J. S.P.N. performed all WGS and CH-associated mutation analyses and managed all genomic data and deposition, supervised by L.B.A. and C.H.M.J. C.E. and P.C. performed scTE and scRNA-seq analyses, supervised by C.H.M.J. P.M. collated all radiation data. K.M., J. Stoudemire, S.R.M., and C.H.M.J. secured funding for this study. J.P., K.M., I.v.d.W., and C.H.M.J. wrote the manuscript, which was reviewed and edited by all authors. C.H.M.J. supervised all aspects of the project.

DECLARATION OF INTERESTS

C.H.M.J. is a co-founder of Impact Biomedicines and Aspera Biomedicines. C.H.M.J. has received royalties from Forty Seven Inc. S.R.M. is a co-founder of Aspera Biomedicines. K.M. is an employee of Aspera Biomedicines. L.B.A. is a co-founder of IO9. P.M. is an employee of Axiom Space. J.P., S.P.N., L.B., C.E., P.C., K.M., I.v.d.W., E.K., J.S., N.K., A.R., S.R.M., T.W., L.B.A., and C.H.M.J. are named on patents related to this work.

STAR★METHODS

Detailed methods are provided in the online version of this paper and include the following:

- KEY RESOURCES TABLE
- EXPERIMENTAL MODEL AND STUDY PARTICIPANT DETAILS
  - Human Subjects
- METHOD DETAILS
  - Sample Collection and Processing
  - Hematopoietic Stem and Progenitor Cell Purification
  - HSPC and Immune Subpopulation FACS Analysis
  - HSPC Clonogenic and Survival Assays
  - Single-Cell Library Preparation and Deep Sequencing
  - HSPC single cell RNA-seq Analyses
  - Single-cell Transposable Element (scTE) Analyses
  - Nucleic Acid Extraction and Sequencing
  - Whole Genome Sequencing-based Identification of Somatic Mutations
  - Whole Genome Sequencing-based Detection of Space-associated Clonal Hematopoiesis
  - Whole Genome Sequencing Telomere Length and Mitochondrial Copy Number Quantification
  - Whole Genome Somatic Mutation Sequencing Analyses

SUPPLEMENTAL INFORMATION

Supplemental information can be found online at https://doi.org/10.1016/j.stem.2025.11.001.

Received: December 6, 2024
Revised: May 21, 2025
Accepted: November 3, 2025

REFERENCES

1. Jamieson, C.H.M., and Weissman, I.L. (2023). Stem-Cell Aging and Pathways to Precancer Evolution. N. Engl. J. Med. *389*, 1310–1319. https://doi.org/10.1056/NEJMra2304431.
2. Orkin, S.H., and Zon, L.I. (2008). Hematopoiesis: An Evolving Paradigm for Stem Cell Biology. Cell *132*, 631–644. https://doi.org/10.1016/j.cell.2008.01.025.
3. Balandrán, J.C., Lasry, A., and Aifantis, I. (2023). The Role of Inflammation in the Initiation and Progression of Myeloid Neoplasms. Blood Cancer Discov. *4*, 254–266. https://doi.org/10.1158/2643-3230.Bcd-22-0176.
4. Oh, J., Lee, Y.D., and Wagers, A.J. (2014). Stem cell aging: mechanisms, regulators and therapeutic opportunities. Nat. Med. *20*, 870–880. https://doi.org/10.1038/nm.3651.
5. Jaiswal, S., and Ebert, B.L. (2019). Clonal hematopoiesis in human aging and disease. Science *366*, eaan4673. https://doi.org/10.1126/science.aan4673.
6. Austin, R., and Aifantis, I. (2024). Hematopoietic Clonal Evolution Goes Spatial. Blood Cancer Discov. *5*, 139–141. https://doi.org/10.1158/2643-3230.Bcd-24-0057.
7. Cabezas-Wallscheid, N., Klimmeck, D., Hansson, J., Lipka, D.B., Reyes, A., Wang, Q., Weichenhan, D., Lier, A., von Paleske, L., Renders, S., et al. (2014). Identification of Regulatory Networks in HSCs and Their Immediate Progeny via Integrated Proteome, Transcriptome, and DNA Methylome Analysis. Cell Stem Cell *15*, 507–522. https://doi.org/10.1016/j.stem.2014.07.005.
8. Gao, X., Zhang, D., Xu, C., Li, H., Caron, K.M., and Frenette, P.S. (2021). Nociceptive nerves regulate haematopoietic stem cell mobilization. Nature *589*, 591–596. https://doi.org/10.1038/s41586-020-03057-y.
9. Jaiswal, S., Fontanillas, P., Flannick, J., Manning, A., Grauman, P.V., Mar, B.G., Lindsley, R.C., Mermel, C.H., Burtt, N., Chavez, A., et al. (2014). Age-Related Clonal Hematopoiesis Associated with Adverse Outcomes. N. Engl. J. Med. *371*, 2488–2498. https://doi.org/10.1056/NEJMoa1408617.
10. Ramabadran, R., Wang, J.H., Reyes, J.M., Guzman, A.G., Gupta, S., Rosas, C., Brunetti, L., Gundry, M.C., Tovy, A., Long, H., et al. (2023). DNMT3A-coordinated splicing governs the stem state switch towards differentiation in embryonic and haematopoietic stem cells. Nat. Cell Biol. *25*, 528–539. https://doi.org/10.1038/s41556-023-01109-9.
11. LaRocca, T.J., Cavalier, A.N., and Wahl, D. (2020). Repetitive elements as a transcriptomic marker of aging: Evidence in multiple datasets and models. Aging Cell *19*, e13167. https://doi.org/10.1111/acel.13167.
12. Gorbunova, V., Seluanov, A., Mita, P., McKerrow, W., Fenyö, D., Boeke, J.D., Linker, S.B., Gage, F.H., Kreiling, J.A., Petrashen, A.P., et al. (2021). The role of retrotransposable elements in ageing and age-associated diseases. Nature *596*, 43–53. https://doi.org/10.1038/s41586-021-03542-y.
13. Jiang, Q., Isquith, J., Ladel, L., Mark, A., Holm, F., Mason, C., He, Y., Mondala, P., Oliver, I., Pham, J., et al. (2021). Inflammation-driven deaminase deregulation fuels human pre-leukemia stem cell evolution. Cell Rep. *34*, 108670. https://doi.org/10.1016/j.celrep.2020.108670.
14. De Cecco, M., Ito, T., Petrashen, A.P., Elias, A.E., Skvir, N.J., Criscione, S.W., Caligiana, A., Brocculi, G., Adney, E.M., Boeke, J.D., et al. (2019). L1 drives IFN in senescent cells and promotes age-associated inflammation. Nature *566*, 73–78. https://doi.org/10.1038/s41586-018-0784-9.
15. López-Otín, C., Blasco, M.A., Partridge, L., Serrano, M., and Kroemer, G. (2023). Hallmarks of aging: An expanding universe. Cell *186*, 243–278. https://doi.org/10.1016/j.cell.2022.11.001.
16. Rando, T.A., Brunet, A., and Goodell, M.A. (2025). Hallmarks of stem cell aging. Cell Stem Cell *32*, 1038–1054. https://doi.org/10.1016/j.stem.2025.06.004.
17. Chua, B.A., Van Der Werf, I., Jamieson, C., and Signer, R.A.J. (2020). Post-Transcriptional Regulation of Homeostatic, Stressed, and Malignant Stem Cells. Cell Stem Cell *26*, 138–159. https://doi.org/10.1016/j.stem.2020.01.005.
18. Garrett-Bakelman, F.E., Darshi, M., Green, S.J., Gur, R.C., Lin, L., Macias, B.R., McKenna, M.J., Meydan, C., Mishra, T., Nasrini, J., et al. (2019). The NASA Twins Study: A multidimensional analysis of a year-long human spaceflight. Science *364*, eaau8650. https://doi.org/10.1126/science.aau8650.
19. Pham, J., Isquith, J., Balaian, L., Ladel, L., Nandi, S.P., Mack, K., van der Werf, I., Klacking, E., Ruiz, A., Mays, D., et al. (2024). Accelerated Hematopoietic Stem Cell Aging in Space. Preprint at bioRxiv. https://doi.org/10.1101/2024.01.28.577076.
20. Jones, C.W., Overbey, E.G., Lacombe, J., Ecker, A.J., Meydan, C., Ryon, K., Tierney, B., Damle, N., MacKay, M., Afshin, E.E., et al. (2024). Molecular and physiological changes in the SpaceX Inspiration4 civilian crew. Nature *632*, 1155–1164. https://doi.org/10.1038/s41586-024-07648-x.
21. Overbey, E.G., Ryon, K., Kim, J., Tierney, B.T., Klotz, R., Ortiz, V., Mullane, S., Schmidt, J.C., MacKay, M., Damle, N., et al. (2024). Collection of biospecimens from the inspiration4 mission establishes the standards for the space omics and medical atlas (SOMA). Nat. Commun. *15*, 4964. https://doi.org/10.1038/s41467-024-48806-z.
22. Crucian, B., Stowe, R.P., Mehta, S., Quiriarte, H., Pierson, D., and Sams, C. (2015). Alterations in adaptive immunity persist during long-duration spaceflight. npj Microgravity *1*, 15013. https://doi.org/10.1038/npjmgrav.2015.13.
23. Grinfeld, J., Nangalia, J., Baxter, E.J., Wedge, D.C., Angelopoulos, N., Cantrill, R., Godfrey, A.L., Papaemmanuil, E., Gundem, G., MacLean, C., et al. (2018). Classification and Personalized Prognosis in Myeloproliferative Neoplasms. N. Engl. J. Med. *379*, 1416–1430. https://doi.org/10.1056/NEJMoa1716614.
24. Kim, J., Tierney, B.T., Overbey, E.G., Dantas, E., Fuentealba, M., Park, J., Narayanan, S.A., Wu, F., Najjar, D., Chin, C.R., et al. (2024). Single-cell multi-ome and immune profiles of the Inspiration4 crew reveal conserved, cell-type, and sex-specific responses to spaceflight. Nat. Commun. *15*, 4954. https://doi.org/10.1038/s41467-024-49211-2.
25. Wu, F., Du, H., Overbey, E., Kim, J., Makhijani, P., Martin, N., Lerner, C.A., Nguyen, K., Baechle, J., Valentino, T.R., et al. (2024). Single-cell analysis identifies conserved features of immune dysfunction in simulated microgravity and spaceflight. Nat. Commun. *15*, 4795. https://doi.org/10.1038/s41467-023-42013-y.
26. Pham, J., Isquith, J., Balaian, L., Nandi, S.P., Engstrom, C., Mack, K., van der Werf, I., Chang, P., Stoudemire, J., Ladel, L., et al. (2025). Nanobioreactor detection of space-associated hematopoietic stem and progenitor cell aging. Cell Stem Cell *32*, 1403–1420.e8. https://doi.org/10.1016/j.stem.2025.07.013.
27. Zeng, A.G.X., Iacobucci, I., Shah, S., Mitchell, A., Wong, G., Bansal, S., Chen, D., Gao, Q., Kim, H., Kennedy, J.A., et al. (2025). Single-cell Transcriptional Atlas of Human Hematopoiesis Reveals Genetic and Hierarchy-Based Determinants of Aberrant AML Differentiation. Blood

Cancer Discov. *6*, 307–324. https://doi.org/10.1158/2643-3230.Bcd-24-0342.

28. Jiang, Q., Isquith, J., Zipeto, M.A., Diep, R.H., Pham, J., Delos Santos, N., Reynoso, E., Chau, J., Leu, H., Lazzari, E., et al. (2019). Hyper-Editing of Cell-Cycle Regulatory and Tumor Suppressor RNA Promotes Malignant Progenitor Propagation. Cancer Cell *35*, 81–94.e7. https://doi.org/10.1016/j.ccell.2018.11.017.
29. Coller, H.A. (2011). Cell Biology. The Essence of Quiescence. Science *334*, 1074–1075. https://doi.org/10.1126/science.1216242.
30. Forsberg, E.C., Passegué, E., Prohaska, S.S., Wagers, A.J., Koeva, M., Stuart, J.M., and Weissman, I.L. (2010). Molecular Signatures of Quiescent, Mobilized and Leukemia-Initiating Hematopoietic Stem Cells. PLoS One *5*, e8785. https://doi.org/10.1371/journal.pone.0008785.
31. Pietras, E.M., Lakshminarasimhan, R., Techner, J.-M., Fong, S., Flach, J., Binnewies, M., and Passegué, E. (2014). Re-entry into quiescence protects hematopoietic stem cells from the killing effect of chronic exposure to type I interferons. J. Exp. Med. *211*, 245–262. https://doi.org/10.1084/jem.20131043.
32. Wilson, A., Laurenti, E., Oser, G., van der Wath, R.C., Blanco-Bose, W., Jaworski, M., Offner, S., Dunant, C.F., Eshkind, L., Bockamp, E., et al. (2008). Hematopoietic Stem Cells Reversibly Switch from Dormancy to Self-Renewal during Homeostasis and Repair. Cell *135*, 1118–1129. https://doi.org/10.1016/j.cell.2008.10.048.
33. Torres-Montaner, A. (2021). The telomere complex and the origin of the cancer stem cell. Biomark. Res. *9*, 81. https://doi.org/10.1186/s40364-021-00339-z.
34. Brazvan, B., Ebrahimi-Kalan, A., Velaei, K., Mehdipour, A., Aliyari serej, Z., Ebrahimi, A., Ghorbani, M., Cheraghi, O., and Nozad Charoudeh, H. (2018). Telomerase activity and telomere on stem progeny senescence. Biomed. Pharmacother. *102*, 9–17. https://doi.org/10.1016/j.biopha.2018.02.073.
35. Zaug, A.J., Goodrich, K.J., Song, J.J., Sullivan, A.E., and Cech, T.R. (2022). Reconstitution of a telomeric replicon organized by CST. Nature *608*, 819–825. https://doi.org/10.1038/s41586-022-04930-8.
36. Lim, C.J., and Cech, T.R. (2021). Shaping human telomeres: from shelterin and CST complexes to telomeric chromatin organization. Nat. Rev. Mol. Cell Biol. *22*, 283–298. https://doi.org/10.1038/s41580-021-00328-y.
37. Vulliamy, T., Beswick, R., Kirwan, M., Marrone, A., Digweed, M., Walne, A., and Dokal, I. (2008). Mutations in the telomerase component NHP2 cause the premature ageing syndrome dyskeratosis congenita. Proc. Natl. Acad. Sci. USA *105*, 8073–8078. https://doi.org/10.1073/pnas.0800042105.
38. Tyrka, A.R., Carpenter, L.L., Kao, H.-T., Porton, B., Philip, N.S., Ridout, S.J., Ridout, K.K., and Price, L.H. (2015). Association of telomere length and mitochondrial DNA copy number in a community sample of healthy adults. Exp. Gerontol. *66*, 17–20. https://doi.org/10.1016/j.exger.2015.04.002.
39. Moreno-Villanueva, M., Wong, M., Lu, T., Zhang, Y., and Wu, H. (2017). Interplay of space radiation and microgravity in DNA damage and DNA damage response. npj Microgravity *3*, 14. https://doi.org/10.1038/s41526-017-0019-7.
40. Behjati, S., Gundem, G., Wedge, D.C., Roberts, N.D., Tarpey, P.S., Cooke, S.L., Van Loo, P., Alexandrov, L.B., Ramakrishna, M., Davies, H., et al. (2016). Mutational signatures of ionizing radiation in second malignancies. Nat. Commun. *7*, 12605. https://doi.org/10.1038/ncomms12605.
41. Zipeto, M.A., Court, A.C., Sadarangani, A., Delos Santos, N.P., Balaian, L., Chun, H.-J., Pineda, G., Morris, S.R., Mason, C.N., Geron, I., et al. (2016). ADAR1 Activation Drives Leukemia Stem Cell Self-Renewal by Impairing Let-7 Biogenesis. Cell Stem Cell *19*, 177–191. https://doi.org/10.1016/j.stem.2016.05.004.
42. Jiang, Q., Crews, L.A., Barrett, C.L., Chun, H.-J., Court, A.C., Isquith, J.M., Zipeto, M.A., Goff, D.J., Minden, M., Sadarangani, A., et al. (2013). ADAR1 promotes malignant progenitor reprogramming in chronic myeloid leukemia. Proc. Natl. Acad. Sci. USA *110*, 1041–1046. https://doi.org/10.1073/pnas.1213021110.
43. Crews, L.A., Balaian, L., Delos Santos, N.P., Leu, H.S., Court, A.C., Lazzari, E., Sadarangani, A., Zipeto, M.A., La Clair, J.J., Villa, R., et al. (2016). RNA Splicing Modulation Selectively Impairs Leukemia Stem Cell Maintenance in Secondary Human AML. Cell Stem Cell *19*, 599–612. https://doi.org/10.1016/j.stem.2016.08.003.
44. Mencia-Trinchant, N., MacKay, M.J., Chin, C., Afshinnekoo, E., Foox, J., Meydan, C., Butler, D., Mozsary, C., Vernice, N.A., Darby, C., et al. (2020). Clonal Hematopoiesis Before, During, and After Human Spaceflight. Cell Rep. *33*, 108458. https://doi.org/10.1016/j.celrep.2020.108458.
45. Brojakowska, A., Kour, A., Thel, M.C., Park, E., Bisserier, M., Garikipati, V.N.S., Hadri, L., Mills, P.J., Walsh, K., and Goukassian, D.A. (2022). Retrospective analysis of somatic mutations and clonal hematopoiesis in astronauts. Commun. Biol. *5*, 828. https://doi.org/10.1038/s42003-022-03777-z.
46. Pessoa Rodrigues, C., Collins, J.M., Yang, S., Martinez, C., Kim, J.W., Lama, C., Nam, A.S., Alt, C., Lin, C., and Zon, L.I. (2024). Transcripts of repetitive DNA elements signal to block phagocytosis of hematopoietic stem cells. Science *385*, eadn1629. https://doi.org/10.1126/science.adn1629.
47. Phan, J., Chen, B., Zhao, Z., Allies, G., Iannaccone, A., Paul, A., Cansiz, F., Spina, A., Leven, A.-S., Gellhaus, A., et al. (2024). Retrotransposons are co-opted to activate hematopoietic stem cells and erythropoiesis. Science *386*, eado6836. https://doi.org/10.1126/science.ado6836.
48. Mulhall, E.M., Gharpure, A., Lee, R.M., Dubin, A.E., Aaron, J.S., Marshall, K.L., Spencer, K.R., Reiche, M.A., Henderson, S.C., Chew, T.-L., et al. (2023). Direct observation of the conformational states of PIEZO1. Nature *620*, 1117–1125. https://doi.org/10.1038/s41586-023-06427-4.
49. Wu, Y., Gao, Z., Chen, B., Koval, O.M., Singh, M.V., Guan, X., Hund, T.J., Kutschke, W., Sarma, S., Grumbach, I.M., et al. (2009). Calmodulin kinase II is required for fight or flight sinoatrial node physiology. Proc. Natl. Acad. Sci. USA *106*, 5972–5977. https://doi.org/10.1073/pnas.0806422106.
50. Camera, A., Tabetah, M., Castañeda, V., Kim, J., Galsinh, A.S., Haro-Vinueza, A., Salinas, I., Seylani, A., Arif, S., Das, S., et al. (2024). Aging and putative frailty biomarkers are altered by spaceflight. Sci. Rep. *14*, 13098. https://doi.org/10.1038/s41598-024-57948-5.
51. Rossmann, M.P., Dubois, S.M., Agarwal, S., and Zon, L.I. (2021). Mitochondrial function in development and disease. Dis. Model. Mech. *14*, dmm048912. https://doi.org/10.1242/dmm.048912.
52. Luxton, J.J., McKenna, M.J., Lewis, A., Taylor, L.E., George, K.A., Dixit, S.M., Moniz, M., Benegas, W., Mackay, M.J., Mozsary, C., et al. (2020). Telomere Length Dynamics and DNA Damage Responses Associated with Long-Duration Spaceflight. Cell Rep. *33*, 108457. https://doi.org/10.1016/j.celrep.2020.108457.
53. Seita, J., and Weissman, I.L. (2010). Hematopoietic stem cell: self-renewal versus differentiation. Wiley Interdiscip. Rev. Syst. Biol. Med. *2*, 640–653. https://doi.org/10.1002/wsbm.86.
54. Ogawa, M. (1993). Differentiation and Proliferation of Hematopoietic Stem Cells. Blood *81*, 2844–2853. https://doi.org/10.1182/blood.V81.11.2844.2844.
55. Rooney, B.V., Crucian, B.E., Pierson, D.L., Laudenslager, M.L., and Mehta, S.K. (2019). Herpes Virus Reactivation in Astronauts During Spaceflight and Its Application on Earth. Front. Microbiol. *10*, 16. https://doi.org/10.3389/fmicb.2019.00016.
56. Orecchini, E., Frassinelli, L., and Michienzi, A. (2017). Restricting retrotransposons: ADAR1 is another guardian of the human genome. RNA Biol. *14*, 1485–1491. https://doi.org/10.1080/15476286.2017.1341033.
57. Eckerling, A., Ricon-Becker, I., Sorski, L., Sandbank, E., and Ben-Eliyahu, S. (2021). Stress and cancer: mechanisms, significance and future directions. Nat. Rev. Cancer *21*, 767–785. https://doi.org/10.1038/s41568-021-00395-5.

58. Benoit Bouvrette, L.P., Bovaird, S., Blanchette, M., and Lécuyer, E. (2019). oRNAment: a database of putative RNA binding protein target sites in the transcriptomes of model species. Nucleic Acids Res. *48*, D166–D173. https://doi.org/10.1093/nar/gkz986.

59. Mansi, L., Tangaro, M.A., Lo Giudice, C., Flati, T., Kopel, E., Schaffer, A.A., Castrignanò, T., Chillemi, G., Pesole, G., and Picardi, E. (2020). REDIportal: millions of novel A-to-I RNA editing events from thousands of RNAseq experiments. Nucleic Acids Res. *49*, D1012–D1019. https://doi.org/10.1093/nar/gkaa916.

60. Andrews, S. (2024). Fast QC: A quality control tool for high throughput sequence data https://www.bioinformatics.babraham.ac.uk/projects/fastqc/.

61. Pedersen, B.S., and Quinlan, A.R. (2018). Mosdepth: quick coverage calculation for genomes and exomes. Bioinformatics *34*, 867–868. https://doi.org/10.1093/bioinformatics/btx699.

62. McKenna, A., Hanna, M., Banks, E., Sivachenko, A., Cibulskis, K., Kernytsky, A., Garimella, K., Altshuler, D., Gabriel, S., Daly, M., et al. (2010). The Genome Analysis Toolkit: A MapReduce framework for analyzing next-generation DNA sequencing data. Genome Res. *20*, 1297–1303. https://doi.org/10.1101/gr.107524.110.

63. Benjamin, D., Sato, T., Cibulskis, K., Getz, G., Stewart, C., and Lichtenstein, L. (2019). Calling Somatic SNVs and Indels with Mutect2. bioRxiv, 861054. https://doi.org/10.1101/861054.

64. Fan, Y., Xi, L., Hughes, D.S.T., Zhang, J., Zhang, J., Futreal, P.A., Wheeler, D.A., and Wang, W. (2016). MuSE: accounting for tumor heterogeneity using a sample-specific error model improves sensitivity and specificity in mutation calling from sequencing data. Genome Biol. *17*, 178. https://doi.org/10.1186/s13059-016-1029-6.

65. Koboldt, D.C., Zhang, Q., Larson, D.E., Shen, D., McLellan, M.D., Lin, L., Miller, C.A., Mardis, E.R., Ding, L., and Wilson, R.K. (2012). VarScan 2: Somatic mutation and copy number alteration discovery in cancer by exome sequencing. Genome Res. *22*, 568–576. https://doi.org/10.1101/gr.129684.111.

66. Farmery, J.H.R., Smith, M.L.; NIHR BioResource - Rare Diseases, and Lynch, A.G. (2018). Telomerecat: A ploidy-agnostic method for estimating telomere length from whole genome sequencing data. Sci. Rep. *8*, 1300. https://doi.org/10.1038/s41598-017-14403-y.

67. Qian, Y., Butler, T.J., Opsahl-Ong, K., Giroux, N.S., Sidore, C., Nagaraja, R., Cucca, F., Ferrucci, L., Abecasis, G.R., Schlessinger, D., et al. (2017). fastMitoCalc: an ultra-fast program to estimate mitochondrial DNA copy number from whole-genome sequences. Bioinformatics *33*, 1399–1401. https://doi.org/10.1093/bioinformatics/btw835.

68. Bergstrom, E.N., Huang, M.N., Mahto, U., Barnes, M., Stratton, M.R., Rozen, S.G., and Alexandrov, L.B. (2019). SigProfilerMatrixGenerator: a tool for visualizing and exploring patterns of small mutational events. BMC Genomics *20*, 685. https://doi.org/10.1186/s12864-019-6041-2.

69. Cyriac Kandoth, J.G., Kandoth, C., Gao, J., qwangmsk, Mattioni, M., Struck, A., Boursin, Y., Penson, A., and Chavan, S. (2018). mskcc/vcf2maf: vcf2maf. (v1.6.16). https://doi.org/10.5281/zenodo.1185418.

70. Mayakonda, A., Lin, D.C., Assenov, Y., Plass, C., and Koeffler, H.P. (2018). Maftools: efficient and comprehensive analysis of somatic variants in cancer. Genome Res. *28*, 1747–1756. https://doi.org/10.1101/gr.239244.118.

71. Dobin, A., Davis, C.A., Schlesinger, F., Drenkow, J., Zaleski, C., Jha, S., Batut, P., Chaisson, M., and Gingeras, T.R. (2012). STAR: ultrafast universal RNA-seq aligner. Bioinformatics *29*, 15–21. https://doi.org/10.1093/bioinformatics/bts635.

72. Li, B., and Dewey, C.N. (2011). RSEM: accurate transcript quantification from RNA-Seq data with or without a reference genome. BMC Bioinform. *12*, 323. https://doi.org/10.1186/1471-2105-12-323.

73. Robinson, M.D., McCarthy, D.J., and Smyth, G.K. (2009). edgeR: a Bioconductor package for differential expression analysis of digital gene expression data. Bioinformatics *26*, 139–140. https://doi.org/10.1093/bioinformatics/btp616.

74. Ritchie, M.E., Phipson, B., Wu, D., Hu, Y., Law, C.W., Shi, W., and Smyth, G.K. (2015). limma powers differential expression analyses for RNA-sequencing and microarray studies. Nucleic Acids Res. *43*, e47. https://doi.org/10.1093/nar/gkv007.

75. Law, C.W., Chen, Y., Shi, W., and Smyth, G.K. (2014). voom: precision weights unlock linear model analysis tools for RNA-seq read counts. Genome Biol. *15*, R29. https://doi.org/10.1186/gb-2014-15-2-r29.

76. Liao, Y., Wang, J., Jaehnig, E.J., Shi, Z., and Zhang, B. (2019). WebGestalt 2019: gene set analysis toolkit with revamped UIs and APIs. Nucleic Acids Res. *47*, W199–W205. https://doi.org/10.1093/nar/gkz401.

77. Hänzelmann, S., Castelo, R., and Guinney, J. (2013). GSVA: gene set variation analysis for microarray and RNA-Seq data. BMC Bioinformatics *14*, 7. https://doi.org/10.1186/1471-2105-14-7.

78. Kolberg, L., Raudvere, U., Kuzmin, I., Vilo, J., and Peterson, H. (2020). gprofiler2 – an R package for gene list functional enrichment analysis and namespace conversion toolset g:Profiler [version 2; peer review: 2 approved]. F1000Research *9*. https://doi.org/10.12688/f1000research.24956.2.

79. Raudvere, U., Kolberg, L., Kuzmin, I., Arak, T., Adler, P., Peterson, H., and Vilo, J. (2019). g:Profiler: a web server for functional enrichment analysis and conversions of gene lists (2019 update). Nucleic Acids Res. *47*, W191–W198. https://doi.org/10.1093/nar/gkz369.

80. Shen, S., Park, J.W., Lu, Z.-x., Lin, L., Henry, M.D., Wu, Y.N., Zhou, Q., and Xing, Y. (2014). rMATS: Robust and flexible detection of differential alternative splicing from replicate RNA-Seq data. Proceedings of the National Academy of Sciences *111*, E5593–E5601. https://doi.org/10.1073/pnas.1419161111.

81. Picardi, E., and Pesole, G. (2013). REDItools: high-throughput RNA editing detection made easy. Bioinformatics *29*, 1813–1814. https://doi.org/10.1093/bioinformatics/btt287.

82. Danecek, P., Bonfield, J.K., Liddle, J., Marshall, J., Ohan, V., Pollard, M.O., Whitwham, A., Keane, T., McCarthy, S.A., Davies, R.M., et al. (2021). Twelve years of SAMtools and BCFtools. GigaScience *10*, giab008. https://doi.org/10.1093/gigascience/giab008.

83. He, J., Babarinde, I.A., Sun, L., Xu, S., Chen, R., Shi, J., Wei, Y., Li, Y., Ma, G., Zhuang, Q., et al. (2021). Identifying transposable element expression dynamics and heterogeneity during development at the single-cell level with a processing pipeline scTE. Nat. Commun. *12*, 1456. https://doi.org/10.1038/s41467-021-21808-x.

84. Hao, Y., Hao, S., Andersen-Nissen, E., Mauck, W.M., Zheng, S., Butler, A., Lee, M.J., Wilk, A.J., Darby, C., Zager, M., et al. (2021). Integrated analysis of multimodal single-cell data. Cell *184*, 3573–3587.e29. https://doi.org/10.1016/j.cell.2021.04.048.

85. Zheng, G.X.Y., Terry, J.M., Belgrader, P., Ryvkin, P., Bent, Z.W., Wilson, R., Ziraldo, S.B., Wheeler, T.D., McDermott, G.P., Zhu, J., et al. (2017). Massively parallel digital transcriptional profiling of single cells. Nature Communications *8*, 14049. https://doi.org/10.1038/ncomms14049.

86. Finak, G., McDavid, A., Yajima, M., Deng, J., Gersuk, V., Shalek, A.K., Slichter, C.K., Miller, H.W., McElrath, M.J., Prlic, M., et al. (2015). MAST: a flexible statistical framework for assessing transcriptional changes and characterizing heterogeneity in single-cell RNA sequencing data. Genome Biol. *16*, 278. https://doi.org/10.1186/s13059-015-0844-5.

87. Korotkevich, G., Sukhov, V., Budin, N., Shpak, B., Artyomov, M.N., and Sergushichev, A. (2021). Fast gene set enrichment analysis. Preprint at bioRxiv. https://doi.org/10.1101/060012.

88. Dolgalev, I. (2022). msigdbr: MSigDB Gene Sets for Multiple Organisms in a Tidy Data Format. https://cran.r-project.org/web/packages/msigdbr/msigdbr.pdf.

89. Yu, G. (2024). enrichplot: Visualization of Functional Enrichment Result.

90. McGinnis, C.S., Murrow, L.M., and Gartner, Z.J. (2019). DoubletFinder: Doublet Detection in Single-Cell RNA Sequencing Data Using Artificial

Nearest Neighbors. Cell Syst. *8*, 329–337.e4. https://doi.org/10.1016/j.cels.2019.03.003.

91. Chen, E.Y., Tan, C.M., Kou, Y., Duan, Q., Wang, Z., Meirelles, G.V., Clark, N.R., and Ma'ayan, A. (2013). Enrichr: interactive and collaborative HTML5 gene list enrichment analysis tool. BMC Bioinform. *14*, 128. https://doi.org/10.1186/1471-2105-14-128.
92. Love, M.I., Huber, W., and Anders, S. (2014). Moderated estimation of fold change and dispersion for RNA-seq data with DESeq2. Genome Biol. *15*, 550. https://doi.org/10.1186/s13059-014-0550-8.
93. Aran, D., Looney, A.P., Liu, L., Wu, E., Fong, V., Hsu, A., Chak, S., Naikawadi, R.P., Wolters, P.J., Abate, A.R., et al. (2019). Reference-based analysis of lung single-cell sequencing reveals a transitional profibrotic macrophage. Nat. Immunol. *20*, 163–172. https://doi.org/10.1038/s41590-018-0276-y.
94. Ianevski, A., Giri, A.K., and Aittokallio, T. (2022). Fully-automated and ultra-fast cell-type identification using specific marker combinations from single-cell transcriptomic data. Nat. Commun. *13*, 1246. https://doi.org/10.1038/s41467-022-28803-w.
95. Goff, D.J., Court Recart, A.C., Sadarangani, A., Chun, H.-J., Barrett, C.L., Krajewska, M., Leu, H., Low-Marchelli, J., Ma, W., Shih, A.Y., et al. (2013). A Pan-BCL2 Inhibitor Renders Bone-Marrow-Resident Human Leukemia Stem Cells Sensitive to Tyrosine Kinase Inhibition. Cell Stem Cell *12*, 316–328. https://doi.org/10.1016/j.stem.2012.12.011.
96. Kuleshov, M.V., Jones, M.R., Rouillard, A.D., Fernandez, N.F., Duan, Q., Wang, Z., Koplev, S., Jenkins, S.L., Jagodnik, K.M., Lachmann, A., et al. (2016). Enrichr: a comprehensive gene set enrichment analysis web server 2016 update. Nucleic Acids Res. *44*, W90–W97. https://doi.org/10.1093/nar/gkw377.
97. Xie, Z., Bailey, A., Kuleshov, M.V., Clarke, D.J.B., Evangelista, J.E., Jenkins, S.L., Lachmann, A., Wojciechowicz, M.L., Kropiwnicki, E., Jagodnik, K.M., et al. (2021). Gene Set Knowledge Discovery with Enrichr. Curr. Protoc. *1*, e90. https://doi.org/10.1002/cpz1.90.
98. Subramanian, A., Tamayo, P., Mootha, V.K., Mukherjee, S., Ebert, B.L., Gillette, M.A., Paulovich, A., Pomeroy, S.L., Golub, T.R., Lander, E.S., et al. (2005). Gene set enrichment analysis: A knowledge-based approach for interpreting genome-wide expression profiles. Proc. Natl. Acad. Sci. USA *102*, 15545–15550. https://doi.org/10.1073/pnas.0506580102.
99. Li, H., Handsaker, B., Wysoker, A., Fennell, T., Ruan, J., Homer, N., Marth, G., Abecasis, G., and Durbin, R.; 1000 Genome Project Data Processing Subgroup (2009). The Sequence Alignment/Map format and SAMtools. Bioinformatics *25*, 2078–2079. https://doi.org/10.1093/bioinformatics/btp352.
100. Jurka, J. (2000). Repbase Update: a database and an electronic journal of repetitive elements. Trends Genet. *16*, 418–420. https://doi.org/10.1016/S0168-9525(00)02093-X.
101. Aaltonen, L.A., Abascal, F., Abeshouse, A., Aburatani, H., Adams, D.J., Agrawal, N., Ahn, K.S., Ahn, S.-M., Aikata, H., and Akbani, R. (2020). Pan-cancer analysis of whole genomes. Nature *578*, 82–93. https://doi.org/10.1038/s41586-020-1969-6.
102. Andrews, S. (2024). Fast QC: A quality control tool for high throughput sequence data. https://www.bioinformatics.babraham.ac.uk/projects/fastqc/.
103. Bergmann, E.A., Chen, B.-J., Arora, K., Vacic, V., and Zody, M.C. (2016). Conpair: concordance and contamination estimator for matched tumor–normal pairs. Bioinformatics *32*, 3196–3198. https://doi.org/10.1093/bioinformatics/btw389.
104. Kim, S., Scheffler, K., Halpern, A.L., Bekritsky, M.A., Noh, E., Källberg, M., Chen, X., Kim, Y., Beyter, D., Krusche, P., et al. (2018). Strelka2: fast and accurate calling of germline and somatic variants. Nat. Methods *15*, 591–594. https://doi.org/10.1038/s41592-018-0051-x.
105. Wingett, S.W., and Andrews, S. (2018). FastQ Screen: A tool for multi-genome mapping and quality control [version 2; peer review: 4 approved]. F1000Res *7*, 7. https://doi.org/10.12688/f1000research.15931.2.
106. Milacic, M., Beavers, D., Conley, P., Gong, C., Gillespie, M., Griss, J., Haw, R., Jassal, B., Matthews, L., May, B., et al. (2024). The Reactome Pathway Knowledgebase 2024. Nucleic Acids Res. *52*, D672–D678. https://doi.org/10.1093/nar/gkad1025.
107. van der Werf, I., Mondala, P.K., Steel, S.K., Balaian, L., Ladel, L., Mason, C.N., Diep, R.H., Pham, J., Cloos, J., Kaspers, G.J.L., et al. (2023). Detection and targeting of splicing deregulation in pediatric acute myeloid leukemia stem cells. Cell Rep. Med. *4*, 100962. https://doi.org/10.1016/j.xcrm.2023.100962.
108. Subread (2023). Subread Package. https://subread.sourceforge.net/.
109. ISB Repeat Masker (2023). Human [Homo sapiens] Genomic Dataset. https://www.repeatmasker.org/species/hg.html.

Please cite this article in press as: Pham et al., Space-associated stem cell hallmarks of aging and resilience in astronauts, Cell Stem Cell (2025), https://doi.org/10.1016/j.stem.2025.11.001

CellPress
OPEN ACCESS

STAR★METHODS

KEY RESOURCES TABLE

REAGENT or RESOURCE	SOURCE	IDENTIFIER
Antibodies		
Anti-human CD45 BV510	BD Biosciences	Cat# 563204; RRID: AB_2738067
Anti-human CD34 BV421	Biolegend	Cat# 343610; RRID: AB_2561358
Anti-human CD3 FITC	Biolegend	Cat# 300306; RRID: AB_314042
Anti-human CD56 BUV737	BD	Cat# 612767; RRID: AB_2860005
Anti-human CD19 APC-Cy7	Biolegend	Cat# 302218; RRID: AB_314248
Anti-human CD14 PE-Cy7	Biolegend	Cat# 301814; RRID: AB_389353
Anti-human CD16 APC	Biolegend	Cat# 302012; RRID: AB_314212
Anti-human CD4 BUV395	BD	Cat# 563552; RRID: AB_2738275
Anti-human CD8 BV711	Biolegend	Cat# 301043; RRID: AB_11218793
Anti-human CD25 PE-Cy7	Biolegend	Cat# 302612; RRID: AB_314282
Anti-human CD127 BV605	Biolegend	Cat# 351333; RRID: AB_2562019
Anti-human CD69 BV650	Biolegend	Cat# 310934; RRID: AB_2563158
Anti-human CD45RA PE	Biolegend	Cat# 304108; RRID: AB_314412
Anti-human CD45RO BV421	Biolegend	Cat# 304224; RRID: AB_2563817
Anti-human CD62L APC-Cy7	Biolegend	Cat# 304814; RRID: AB_493582
Anti-human CD27 APC	Biolegend	Cat# 356410; RRID: AB_2561957
Anti-human CCR7 AF700	Biolegend	Cat# 353244; RRID: AB_2617001
7-AAD Viability Staining Solution	Biolegend	Cat. 420404
FcR Blocking Reagent, human	Miltenyi	Cat. 130-059-901
Biological Samples		
Peripheral Blood	Obtained through patient consenting according to the Institutional Review Board-approved protocols by NASA and UC San Diego.	N/A
Critical Commercial Assays		
CD34 MicroBead Kit, UltraPure, human	Miltenyi Biotec	Cat# 130-100-453
UltraComp beads	Thermo Fisher Scientific	Cat# 01-3333-42
RNeasy Micro Kit	Qiagen	Cat# 74004
DNeasy Blood and Tissue Kit	Qiagen	Cat# 69504
MethoCultTM H4330	Stem Cell Technologies	Cat# 04330
RLT Buffer	Qiagen	Cat# 79216
Chromium Next GEM Single Cell 3' GEM, Library & Gel Bead Kit v3.1	10X Genomics	Cat# PN-1000121
Chromium Next GEM Chip G Single Cell Kit	10X Genomics	Cat# PN-1000120
Single Index Kit T Set A	10X Genomics	Cat# PN-1000213
NovaSeq 6000 S4 Reagent it v1.5 (200 cycles)	Illumina	Cat# 20028313
NextSeq 2000 P3 Reagents (300 cycles)	Illumina	Cat# 20040561
NEBNext DNA Library Prep Kit	New England Biolabs	Cat# E7645
Rapid Plus DNA Lib Prep Kit	Abclonal Technology	Cat# RK20208
LEGENDplex Human Hematopoietic Stem Cell panel	Biolegend	Cat# 740611
LEGENDplex Human Inflammation Panel 1	Biolegend	Cat# 740809

(*Continued on next page*)

Please cite this article in press as: Pham et al., Space-associated stem cell hallmarks of aging and resilience in astronauts, Cell Stem Cell (2025), https://doi.org/10.1016/j.stem.2025.11.001

Continued

REAGENT or RESOURCE	SOURCE	IDENTIFIER
Deposited Data		
RNA-sequencing dataset	This paper	dbGaP: phs004267.v1.p1
scRNA-sequencing dataset	This paper	dbGaP: phs004267.v1.p1
Analysis codes	This paper	https://github.com/AlexandrovLab/EnsembleVariantCallingPipeline; https://doi.org/10.5281/zenodo.16413670
Databases/References Datasets		
Hg38 Fasta	GRCh38.d1.vd1	GDC Reference Files
oRNAment	Benoit et al.[58]	http://rnabiology.ircm.qc.ca/BIF/oRNAment/static/Homo_sapiens_cDNA_oRNAment.csv.gz
REDIportal.80	Mansi et al.[59]	http://srv00.recas.ba.infn.it/webshare/ATLAS/donwload/TABLE1_hg19.txt.gz
dbSNP		https://ftp.ncbi.nih.gov/snp/redesign/latest_release/VCF/GCF_000001405.39.gz
Software and Algorithms		
FastQC (Version 0.12.0)	Andrews[60]	https://www.bioinformatics.babraham.ac.uk/projects/fastqc/
Mosdepth (Version 0.3.4)	Pedersen and Quinlan[61]	https://github.com/brentp/mosdepth
GATK (Version 4.0.11.0)	McKenna et al.[62]	https://www.broadinstitute.org/gsa/wiki/index.php/The_Genome_Analysis_Toolkit
Mutect2	Benjamin et al.[63]	https://gatk.broadinstitute.org/hc/en-us/articles/360037593851-Mutect2
Strelka2	Fan et al.[64]	https://github.com/Illumina/strelka
Varscan2	Koboldt et al.[65]	https://dkoboldt.github.io/varscan/
MuSE2	Fan et al.[64]	https://bioinformatics.mdanderson.org/public-software/muse/
Telomerecat	Farmery et al.[66]	https://github.com/cancerit/telomerecat
FastMitoCalc	Qian et al.[67]	https://github.com/HSGU-NIA/mitoAnalyzer
SigProfilerMatrixGenerator (Version 1.2.16)	Bergstrom et al.[68]	https://github.com/AlexandrovLab/SigProfilerMatrixGenerator
SigProfilerPlotting (Version 1.3.13)	Bergstrom et al.[68]	https://github.com/AlexandrovLab/SigProfilerPlotting
Vc2maf (Version 1.6.19)	Cyriac Kandoth et al.[69]	https://github.com/mskcc/vcf2maf
Maftools R Bioconductor	Mayakonda et al.[70]	https://bioconductor.org/packages/release/bioc/html/maftools.html
STAR (Version 2.5.3a)	Dobin et al.[71]	https://github.com/alexdobin/STAR
RSEM (Version 1.3.0)	Li and Dewey[72]	https://deweylab.github.io/RSEM/
GENCODE		https://www.gencodegenes.org/human/release_19.html
EdgeR	Robinson et al.[73]	http://bioconductor.org/packages/release/bioc/html/edgeR.html
Limma	Ritchie et al.[74]	https://www.bioconductor.org/packages/release/bioc/html/limma.html
Limma-voom	Law et al.[75]	https://www.bioconductor.org/packages/release/bioc/html/limma.html
webGestalt	Liao et al.[76]	http://www.webgestalt.org/
GSVA	Hänzelmann et al.[77]	https://bioconductor.org/packages/release/bioc/html/GSVA.html
gProfiler	Kolberg et al.[78]; Raudvere et al.[79]	https://biit.cs.ut.ee/gprofiler/page/r
rMATS turbo	Shen et al.[80]	https://github.com/Xinglab/rmats-turbo
REDItools	Picardi and Pesole[81]	http://srv00.recas.ba.infn.it/reditools/

(*Continued on next page*)

Please cite this article in press as: Pham et al., Space-associated stem cell hallmarks of aging and resilience in astronauts, Cell Stem Cell (2025), https://doi.org/10.1016/j.stem.2025.11.001

Continued

REAGENT or RESOURCE	SOURCE	IDENTIFIER
RepeatMasker		https://www.repeatmasker.org/
Bcl2fastq (Version 2.17)		https://support.illumina.com/sequencing/sequencing_software/bcl2fastq-conversion-software.html
SAMtools (Version 1.20)	Danecek et al.[82]	https://github.com/samtools/samtools
scTE (Version 1.0)	He et al.[83]	https://github.com/JiekaiLab/scTE/tree/master
SeuratDisk		https://mojaveazure.github.io/seurat-disk/index.html
Seurat	Hao et al.[84]; https://satijalab.org/seurat/authors#citation	https://satijalab.org/seurat/
Azimuth	Hao et al.[84]	https://azimuth.hubmapconsortium.org/
Cell Ranger	Zheng et al.[85]	https://www.10xgenomics.com/support/software/cell-ranger/latest
MAST	Finak et al.[86]	https://rglab.github.io/MAST/
Fgsea	Korotkevich et al.[87]	https://github.com/ctlab/fgsea?tab=readme-ov-file
msigdbr	Dolgalev et al.[88]	https://igordot.github.io/msigdbr/
enrichplot	Yu et al.[89]	https://github.com/YuLab-SMU/enrichplot
DoubletFinder	McGinnis et al.[90]	https://github.com/chris-mcginnis-ucsf/DoubletFinder
Enrichr	Chen et al.[91]	https://maayanlab.cloud/Enrichr/
DESeq2	Love et al.[92]	https://github.com/thelovelab/DESeq2
SingleR	Aran et al.[93]	https://github.com/dviraran/SingleR
scType	Ianevski et al.[94]	https://github.com/IanevskiAleksandr/sc-type
FlowJo	FLOW JO LLC	https://www.flowjo.com/
LEGENDplex Qognit	Biolegend	N/A
GraphPad Prism	GraphPad Software Inc.	https://www.graphpad.com/scientific-software/prism/
Microsoft Excel	Microsoft	N/A
Equipment and Instruments		
BD-Fortessa X-20	UCSD Human Embryonic Stem Cell Core Facility	N/A
Chromium Controller	Salk Institute Next Generation Sequencing Core Facility	N/A
Chromium X	UCSD gCore	N/A
NextSeq 2000	Scripps Research Genomics Core	N/A
NovaSeq 6000	Salk Institute Next Generation Sequencing Core Facility	N/A
NovaSeq X Plus	Salk Institute Next Generation Sequencing Core Facility	N/A

EXPERIMENTAL MODEL AND STUDY PARTICIPANT DETAILS

Human Subjects

Primary patient peripheral blood samples were obtained from consenting astronauts at Axiom Space Inc. according to NASA and UC San Diego Institutional Review Board-approved protocols.

METHOD DETAILS

Sample Collection and Processing

Peripheral blood (PB) from consenting individuals (N=9) as part of NASA IRB study 0547 was collected from 6 timepoints, L-30 ± 20 days, L-1 ± 10 days, Inflight ± 10 days, R+1 ± 10 days, R+30 ± 60 days, and R+1 year. One additional pre-flight timepoint

(L-18 days) was collected for Ax-4 individuals due to launch slips. All PB samples were delivered to Sanford Consortium for Regenerative Medicine (2880 Torrey Pines Scenic Drive, La Jolla, CA 92037) and processed under BSL2 conditions within 24-96 hours of venipuncture. Depending on shipping duration, samples were either shipped at ambient temperature (within 24-hrs of vein contact), or with ice gel packs (>24-hrs of vein contact). Upon receipt of samples, peripheral blood mononuclear cells (PBMCs) were isolated by Ficoll Paque (density 1.077 g/mL) density centrifugation. Samples were diluted 1:3.5 in HBSS to a total volume of 35mL prior to underlaying Ficoll. Prepared samples were centrifuged for 20 minutes at 1500 RPM and 20°C without deceleration. The PBMCs were collected and washed twice with HBSS prior to proceeding with downstream experiments.

Hematopoietic Stem and Progenitor Cell Purification

Pelleted PBMCs were resuspended in 300uL of cold staining media (HBSS with 2% FBS). 100uL of both CD34+microbeads (130-100-453, Miltenyi Biotec) and FcR Human Blocking Reagent (130-059-901, Miltenyi Biotec) were added to the resuspended cells and allowed to incubate in darkness for 30 minutes on ice. 10mL of staining media was added to the incubation mixture and spun at 1100rpm for 3 minutes at 4°C. After aspirating the supernatant, the pellet was resuspended in 1mL of staining media and filtered through a Blue Top Round Bottom Falcon Tube (08-771-23, Falcon). As the cells filtered through the Falcon tube, 500uL of staining media was used to wet an MS Column (130-042-201, Miltenyi Biotec). To separate the CD34+ population from its negative fraction, the cells were pipetted into the MS column, where the CD34- filtrate was collected. Once the filtrate ran through the column, the column was washed three times in 1 mL of staining media. When the staining media had fully eluted out of the MS column, the column was placed atop a new collection tube. 1mL of staining media was then added to the column and plunged through the column with force and in quick succession to obtain the isolated CD34+ population.

HSPC and Immune Subpopulation FACS Analysis

All flow cytometry stains were performed in HBSS/2% FBS for 20 min on ice. FcR Blocking Reagent (Miltenyi, cat. 130-059-901) was added to all samples at a 1:50 dilution for 10 minutes on ice prior to antibody staining. 7-AAD viability staining solution (Biolegend, cat. 420404) was included in the antibody staining mixture at a 1:50 dilution for all samples. Each sample was split in half and stained with two immunophenotyping panels. Panel 1 contained CD45 BV510, CD34 BV421, CD3 FITC, CD56 BUV737, CD19 APC-Cy7, CD14 PE-Cy7, CD16 APC, and 7-AAD viability staining solution. Panel 2 contained CD45 BV510, CD3 FITC, CD4 BUV737, CD8 BV711, CD25 PE-Cy7, CD127 BV605, CD69 BV650, CD45RA PE, CD45RO BV421, CD62L APC-Cy7, CD27 APC, CCR7, AF700, and 7-AAD viability staining solution. Analysis was performed on a LSRFortessa X-20 or LSR II instrument at the UC San Diego Human Embryonic Stem Cell Core and Salk Institute for Biological Studies Flow Cytometry Core Facility respectively. FlowJo software was used for analysis of cell populations. For all analyses 7-AAD+ cells were gated out, and single cells were gated based on FSC-H vs FSC-A. Statistical significance was determined using a two-tailed t-test of unequal variance. P-values less than 0.05 were considered significant.

HSPC Clonogenic and Survival Assays

Clonogenic experiments were performed as previously described.[95] Briefly, CD34+ cells were resuspended in fresh media and plated in methylcellulose (MC) in triplicate (Stemcell Technologies, catalog H4335). After 2 weeks, the primary colony (survival assay) clusters of more than 40 cells were counted and individual multilineage colonies were plucked, cells resuspended and re-plated again in fresh MC. Secondary colonies (self-renewal assay) were counted after another 14 days. In survival assays, total number of colonies was considered to be 100% and results are presented as percent of change. In self-renewal assays, the data represents the percent of replated colonies. Error bars indicate the SE of triplicate. Statistical analysis comprised Student's t-test and one-way Anova, including All Pairwise Multiple Comparison Procedures (Holm-Sidak method).

Single-Cell Library Preparation and Deep Sequencing

After selection, CD34-positive and CD34-negative fractions were either separately aliquoted or re-combined at a specific ratio determined by available cell number. Aliquots of 10,000 cells were resuspended at 1000 cells per uL in sterile filtered 0.04% BSA in PBS. For higher cell yields (CD34- fraction), 35,000 cells were resuspended at 1000 cells per uL in 0.04% BSA in PBS. Single-cell libraries were prepared using 10X-3' v3.1 Gene Expression (10X Genomics) kit as per manufacturer's instruction. The libraries' quality and quantity were assessed using the TapeStation 4200 DNA High Sensitivity analysis and the Qubit 4 dsDNA high sensitivity assay, pooled and sequenced on the Illumina NovaSeq 6000 platform (Next Generation Sequencing Core, Salk Institute, La Jolla, CA, USA) using S4 flow cells (sequencing depth PE200) and 1% PhiX. For each sample, a custom calculation was done to assign a maximum number of reads based on the percentage of HSC present in the original sample resulting in range of 60 M to 500 M reads per sample.

HSPC single cell RNA-seq Analyses

Sequenced reads from each GEX library generated were aligned to the human reference genome GRCh38, downloaded from the 10X genomics website (10X Genomics, GRCh38-2020-A), and annotated with Ensembl release 98. Quality control, alignment, and quantification of reads were performed using the Cell Ranger v.7.1.0 (10X Genomics) 'count' pipeline, generating count matrices that filtered out empty droplets.

Please cite this article in press as: Pham et al., Space-associated stem cell hallmarks of aging and resilience in astronauts, Cell Stem Cell (2025), https://doi.org/10.1016/j.stem.2025.11.001

GEX count matrices were loaded with Seurat v.5.1.0 (Satija Lab)[84] and individual datasets were bioinformatically cleaned for doublets using DoubletFinder v2.0.4.[90] Then, count matrices were merged into a single object and filtered for cells with outlier UMI counts (low quality cells and doublets), high mitochondrial gene expression (due to cellular stress or loss of cytoplasmic RNA), and low number of sequenced genes. Molecular count data for each sample were individually log normalized and scaled in Seurat with the additional steps of regressing UMI counts, and gene counts during scaling to mitigate their effects on dimensionally reduced clustering. Highly variable genes were identified as the union of the top 3,000 genes from each sample after normalization, and then used to calculate principal components using RunPCA. Normalized and scaled samples were integrated using the IntegrateLayers function using the ''scVIIntegration'' method in Seurat.[84]

Visualization and clustering of the integrated object was performed by calculating the PCA for dimensionality reduction visualization using the UMAP function in Seurat (Satija Lab).[84] After identified clusters via FindClusters in Seurat,[84] identities were assigned using SingleR,[93] scType,[94] and Azimuth (Butler A, Darby C, Hao Y, Hartman A, Hoffman P, Molla G, Satija R (2023). *Azimuth: A Shiny App Demonstrating a Query-Reference Mapping Algorithm for Single-Cell Data*. R package version 0.5.0, https://github.com/satijalab/azimuth.) using the Human PBMC reference (Integrated analysis of multimodal single-cell data Hao, Yuhan et al. Cell, Volume 184, Issue 13, 3573 - 3587.e29). Results were verified and corrected using differentially expressed genes calculated through FindAllMarkers in Seurat[84] and Enrichr.[91,96,97]

The CD34+ HSPCs were further classified into 5 clusters using the FindClusters function in Seurat.[2] These clusters were based on CD34 and CD38 gene expression profiles, removing one cluster that was negative for both CD34, CD38, and PTPRC (CD45). Clusters were named as follows: ''CD34+CD38-'', ''CD34+CD38mid'', ''CD34+CD38+'', and ''CD34low''. Differentially expressed genes (DEGs) were calculated using the ''MAST'' algorithm,[86] which is tailored to scRNA-seq data DEG analysis using a model that parameterizes both stochastic dropout and characteristic bimodal expression distributions, for the FindMarkers function of Seurat (min.pct = 0.1, logfc.threshold = 0.25). DEGs from FindMarkers were used to generate ranked gene lists ordered by log-fold change for Gene Set Enrichment Analysis (GSEA) using the fgsea v1.22.0.[87] Fast gene set enrichment analysis[87] package and gene signatures were pulled from the Molecular Signatures Database (MSigDB) using msigdbr v7.5.1[88,89,98] Visualization of GSEA results was performed using the enrichplot v1.16.2 package.[98] Visualization of functional enrichment result was performed using R package (version 4.3.2).

Pseudobulk analysis was performed by starting with the integrated object (above) and extracting the RNA counts and metadata to create a SingleCellExperiment object. The function aggregate Matrix from the Bioconductor[92] package DESeq2was used to create a counts matrix. These data were input into a DESeq2 object, normalized, and log transformed for visualization of specific genes.

Single-cell Transposable Element (scTE) Analyses

The.bam files generated by CellRanger, were filtered using SAMtools[82,99] to remove reads lacking cell barcodes. After filtering, the scTE pipeline[83] was applied to realign reads to known transposable elements (TEs) using UCSC Repeatmasker[100] annotations. Once annotated, the scTE output was generated as a.h5ad file for conversion to h5seurat form in R for further downstream single-cell analysis.

To quantify the expression of predefined LINEs and hERVs lists across single cells, the AddModuleScore function in Seurat (version 5.0) was used to compute the average expression of each gene set (module) on a per-cell basis.

Nucleic Acid Extraction and Sequencing

For DNA, cells were pelleted and frozen at -80°C prior to extraction using the Qiagen DNeasy Blood and Tissue Kit according to manufacturers' protocol (Qiagen, catalog 69504). DNA was eluted with Qiagen Buffer AE. Extracted DNA from these samples was sent to Novogene (Sacramento, CA) for 90x whole genome sequencing. DNA quality control was done using Qubit 4 Fluorometer (Invitrogen) and 4200 Tape Station system (Agilent). DNA sequencing library preparation for Ax-2 samples was performed using the NEBNext® Ultra™ II DNA Library Prep Kit for Illumina® (E7645L) following the manufacturer's recommendations. DNA sequencing library preparation for Ax-3 samples was performed using the Rapid Plus DNA Library Prep Kit (RK20208 ABclonal Technology) following the manufacturer's recommendations. Qualified libraries were paired and sequenced on an Illumina NovaSeq 6000 platform using 150 PE sequencing chemistry to 90x coverage according to effective concentration and data volume. For RNA, cells were lysed in RLT buffer (Qiagen) and 10% beta-mercaptoethanol. Samples were extracted using Qiagen RNeasy Micro Kit according to manufacturers' protocol (Qiagen, catalog 74004). RNA was eluted in RNase-free water and frozen at -80°C until assessed for quality. Samples with RNA integrity number (RIN) >7 were further processed for RNA-sequencing (The Scripps Research Institute Next Generation Sequencing Core). RNA-seq was performed on Illumina's NextSeq 500 sequencer with 150bp paired-end reads.

Whole Genome Sequencing-based Identification of Somatic Mutations

Raw sequence data were downloaded to the Triton Shared Compute Cluster (*San Diego Supercomputer Center (2022): Triton Shared Computing Cluster*. *University of California, San Diego*. *Service*. https://doi.org/10.57873/T34W2R) from ftp server link shared by Novogene (Sacramento, CA). All the post-sequencing analysis was performed within TSCC at UC San Diego. This methodology for identification of somatic mutations from bulk sequencing data follows established approaches from large genomics consortia.[101] Briefly, quality assurance of the raw FASTQ files were evaluated using FastQC (Version 0.12.0) and Mosdepth (Version 0.3.4).[61,102] Raw sequence reads were aligned to the human reference genome GRCh38.d1.vd1. The aligned reads were marked duplicated using MarkDuplicates (Picard) from GATK (Version 4.0.11.0).[62] Concordance between paired samples were checked using Conpiar version

0.2.[103] An ensemble variant calling pipeline (EVC) was used to identify single nucleotide variants (SNV) and short insertions and deletions (indels). EVC implements the SNV and indel variant calling from four variant callers (Mutect2, Strelka2, Varscan2, and MuSE2) and only mutations that are identified by any two variant callers were considered as *bona fide* mutations.[62,64,65,104]

Analysis of mutational profiles was performed using our previously established methodology with the SigProfiler suite of tools used for summarization, simulation, visualization, and assignment of mutational profiles. Briefly, mutational matrixes for SBS, DBS and Indels were generated with SigProfilerMatrixGenerator (Version 1.2.16).[68] Plotting of each mutational profile was done with SigProfilerPlotting (Version 1.3.13).

The mskcc/vcf2maf (*Cyriac Kandoth. mskcc/vcf2maf: vcf2maf v1.6. (2020). doi:10.5281/zenodo.593251*) was used to annotate each mutation with its genomic coordinates using Ensembl Variant Effect Predictor (VEP, v106) and the annotated files were saved as mutation annotation format (MAF). Plotting of the genetic annotation was done using Maftools[70] (version 2.16.0) within R (v4.3.1) statistical language. Annotation of each C>T mutation to its CpG island is done using MutationalPatterns (v3.10.0) packages in R.

Whole Genome Sequencing-based Detection of Space-associated Clonal Hematopoiesis

To identify the mutation affecting clonal hematopoiesis associated drivers, mutations were called using Mutect2 single samples mode by using mark duplicated reads files from EVC pipeline. To identify the mutation affecting clonal hematopoiesis associated drivers, mutations were called using Mutect2 single samples mode by using mark duplicated reads files from EVC pipeline. Due to variations in the DNA library preparation kit and observed differences in allele frequency (AF) distribution from Mutect2 single samples mode call, low AF mutations were filtered out by applying a threshold of AF $\leq$ 10%. Mutations were then filtered using 123 Clonal Hematopoiesis gene's genomic co-ordinates using bcftools version 1.19. Following annotating the mutation with mskcc/vcf2maf, they were filtered with the "AlphaMissense" (Ref, Accurate proteome-wide missense variant effect prediction with AlphaMissense) annotation for "likely pathogenic" mutations based on the pathogenicity score within the tool. "AlphaMissense" annotated matched samples were plotted using Maftools[70] (version 2.16.0) within R (v4.3.1) statistical language.

Whole Genome Sequencing Telomere Length and Mitochondrial Copy Number Quantification

The mark duplicated reads were used for telomere length estimation using Telomerecat[66] (Telomere Computational Analysis Tool). The 'bam2length' parameters were used with simulation sets to 100 and output options set to details parameters. FastMitoCalc[67] tool was employed in order to determine the average mitochondrial DNA copy number by following the parameter descried in the tools methods sections.

Whole Genome Somatic Mutation Sequencing Analyses

Somatic mutations in whole-genome sequencing data were identified using our ensemble variant calling pipeline, which is freely available under the permissive 2-clause BSD license at: https://github.com/AlexandrovLab/EnsembleVariantCallingPipeline. All other computational tools utilized in this publication have been mentioned in the methodology section and can be accessed through their respective publications.

Whole-transcriptome Sequencing (RNA-Seq) Analyses

Bulk RNA-Seq data were processed as previously reported.[18] Briefly, fastq files were processed by the FastQC tool[105] to verify quality. Gene and isoform expression counts tables were generated with STAR RSEM[71,72] using the human reference genome (GRCh38_p13_v43) and GENCODE annotation (gencode.v19.annotation.gtf). Using the Bioconductor packages edgeR[73] and limma[74] samples were merged, filtered, normalized with the trimmed mean of M-values method[73] and transformed with limma-voom prior to limma differential expression analysis comparing the various timepoints. Significance was defined as adjusted p-value < 0.05. Functional enrichment analysis was performed with the Bioconductor package fgsea[87] and the Reactome database as the ontology.[106]

RNA Editome Analyses

RNA editing events within each sample were determined as described previously.[107] ADAR-driven events were the focus of this analysis, so positive strand A to G and negative strand T to C variants were retained for quantification of total edits within each sample group.

Retrotransposon Analyses

The.bam files generated by STAR alignment (described above), along with the repeatmasker.hg38.gtf file (downloaded from the UCSC genome browser), were used as input into the "featureCounts" function from the Subread R package[108] to generate counts of retrotransposons. Counts were aggregated for all samples, filtered, normalized, and converted to log counts per million (lcpm). Retrotransposons were also annotated using the "hg38.fa.out" file.[109] As above, differential expression of retrotransposons was determined using limma.[74]

Cytokine Arrays

Plasma was analyzed using the BioLegend LEGENDplex Human Hematopoietic Stem Cell Panel (IL-6, FLT3L, GM-CSF, IL-3, IL-34, IL-11, SCF, LIF, CXCL12 (SDF-1), IL-15, M-CSF, IL-7; Lot #: B387711) and LEGENDplex Human Inflammation Panel 1 (IL-1b, IFN-a2,

Please cite this article in press as: Pham et al., Space-associated stem cell hallmarks of aging and resilience in astronauts, Cell Stem Cell (2025), https://doi.org/10.1016/j.stem.2025.11.001

IFN-g, TNF-a, MCP-1, IL-6, IL-8, IL-10, IL12p70, IL-17A, IL-18, IL-23, IL-33; Lot #: B408881) kits. Frozen plasma samples were thawed on ice and centrifuged prior to loading into sample wells. Samples were run according to the manufacturer's protocol. Samples were run on the MACSQuant 10 flow cytometer, and the FCS files were uploaded into LEGENDplex's Qognit database for analysis. Concentrations are reported in pg/ml and bar plots done in GraphPad Prism.

QUANTIFICATION AND STATISTICAL ANALYSIS

Statistical Analyses

For clonogenic survival and self-renewal assays, averaged colonies were calculated and graphed with error bars denoting SE or SD, as indicated in individual figure legends. Student's t-test and one-way ANOVA (Holm-Sidak) statistical analyses were performed and described in each figure legend. For flow cytometry analyses, data was graphed and analyzed in GraphPad Prism (San Diego, CA). Statistical significance was determined using a two-tailed t-test of unequal variance. *P*-values less than 0.05 were considered significant. Analyses from sequencing data were graphed and calculated using Microsoft Excel or GraphPad Prism. Statistics were assessed by Student's t-tests, as indicated in the figure legends. Statistics for scRNA-seq analyses were calculated using Mann-Whitney U tests with FDR < 0.05. One-way ANOVA analysis, including Tukey's multiple comparisons test, was used to calculate statistics for cytokine array assays in GraphPad Prism. All statistical significance was determined for p or adjusted p values < 0.05.